A Multi-step Interpolated-FFT procedure for full-field nonlinear modal testing of turbomachinery components

Xing Wang[1,2], Michal Szydlowski[2], Jie Yuan[2], Christoph Schwingshackl[2]

[1]School of Aeronautics and Astronautics, Sun Yat-sen University (Shenzhen Campus), Shenzhen, China.

[2]Department of Mechanical Engineering, Imperial College London, London, United Kingdom.

Abstract

Model updating for lightweight structures featuring geometrical nonlinearities has long been a goal in the aerospace industry, which requires spatially detailed measurement of the structure vibrating at large amplitudes. Performing such a measurement for lightweight structure is an extremely challenging task due to its low mass-to-area ratio, complex spatial deformation shapes, and geometrically nonlinear behaviours. Indeed, the current full-field measurements of nonlinear structural dynamics are mostly limited to flat, small-scale, academic structures such as beams or plates. To enable full-field measurement of nonlinear responses of large-scale industrial structures, a procedure based on the Three-Dimensional Scanning Laser Doppler Vibrometry (3D SLDV) is developed in this paper, in which full-field, multi-harmonic operating deflection shapes are measured when the structure is vibrating at its resonance. More specifically, a super-short sampling interval is used for each scan point to achieve a significant reduction in measurement duration. A novel Multi-step Interpolated-Fast Fourier Transform (Multi-step Interpolated-FFT) procedure is proposed to refine the coarse frequency resolution and suppress the severe spectral leakage of the signal spectra. In the procedure, the instantaneous driving frequency is first interpolated using the force signal and then used to perform a fixed-frequency interpolation for each harmonic of the response signals. In such a way, it allows accurate estimations of the frequencies, magnitudes and phase lags of the constituent harmonics in the measured signal sets. Numerical validations of the proposed procedure are carried out to investigate its accuracy and robustness with regard to different signal frequencies and noise levels before it is

applied to experimental data of an industrial-scale fan blade. Results have shown that it allows, for the first time, to capture full-field, multi-harmonic operating deflection shapes of a large-scale, geometrically-nonlinear structure vibrating at its resonance. These spatially-detailed operating deflection shapes are advantages in describing local deformation patterns of a nonlinear structure, allowing essential ingredients in model updating algorithms, such as the Modal Assurance Criterion (MAC) values, to be correlated with exceptionally high quality.

Keywords: geometrical nonlinearity, full-field dynamic testing, interpolated fast Fourier transform, turbomachinery component.

1. Introduction

Demands to improve fuel efficiency and reduce environmental impacts of aero engines have led to ever more flexible blade designs that can experience considerable deformations during operation [1,2]. As a result, geometric nonlinearities are present in the blade dynamics, and multiple harmonics are found in the responses even when the structure is excited mono-harmonically. These harmonics can coincide with higher structural modes, leading to additional responses and potentially causing failures in unexpected areas [3]. Consequently, measuring full-field vibrations of such geometrically nonlinear structures and using the test data to validate numerical models is of the highest interest to an engine manufacturer. Different from the well-established Experimental Modal Analysis (EMA) for linear structures [4], experimental testing of a geometrically nonlinear structure is an extremely challenging task: 1) its dynamics might be significantly modified if conventional 'contact' transducers are used. 2) Its responses contain multiple harmonics even when the structure is excited by a single sinusoidal input. 3) Its resonant frequency may shift with different input levels. As a result, experimental investigations of the dynamics of geometrically nonlinear structures are scarce, rendering further development of model updating techniques even more challenging. Ehrhardt et al. [5,6] presented early works on applications of High-speed Three-dimensional Digital Image Correlation (High-speed 3D DIC) system [5,6] and Continuous Scanning Laser Doppler Vibrometry (CSLDV) [5] to measure the vibrations of geometrically nonlinear structures, where the full-field shapes of higher-order harmonics were captured in addition to the conventional

fundamental harmonic shape of the structure. Nevertheless, these measurement techniques have only been applied to the nonlinear dynamic characterisation of academic structures, such as a beam or a plate. Applications to industrial-scale structures featuring curved geometries still require further research efforts.

This paper considers measuring the dynamic responses of lightweight structures using a Scanning Laser Doppler Vibrometry (SLDV), which is a mature technique in the characterisation of linear structural dynamics. It produces robust, reliable results and has been widely practised by engineers in the industry [1,2,7-13]. For example, the newest version of 3D SLDV (Polytec PSV-500-3D-HV) [9] is capable of automatically measuring full-field, 3D vibrational responses with minimal surface treatment of the test structure due to the use of infrared lasers. It represents an excellent tool to capture the dynamic behaviours of vibrating turbomachinery components [1,2,10,12]. However, 3D SLDV is essentially a single 3D transducer: it dwells at a scan point for a duration and then moves to the next scan point successively. This measurement manner brings many limitations: (i) a long measurement duration is required for a full-field scan, which can be several hours for a dense grid with thousands of points [7,11]. To reduce testing time, Polytec offers the so-called 'FastScan' measurement approach [9] for linear structures, where an open-loop, mono-harmonic voltage is used to drive the shaker, and only the fundamental harmonic components of the responses are estimated. This process would neglect the critical higher-order harmonics that may co-exist in the responses and thus cannot be directly used to measure nonlinear structural responses. The current version of this measurement approach also lacks a module to tune the input force to a desired level or a required phase lag with respect to the structural response, which are essential steps for the quantitative characterisation of nonlinear structural dynamics. (ii) Even with such a long measurement duration, the sampling time interval for each scan point is still quite limited, resulting in a coarse frequency resolution (e.g., several Hz [11]) and a significant amount of energy leakage in the output spectrum if a non-integral number of cycles of the signal is sampled. Tapering the signals with smoothing windows can minimise the spectral leakage; however, it increases the resolution bandwidth and has neglectable effects on the phase estimate accuracy of higher-order harmonics [14-18]. (iii) Measurement of operating deflection shapes using a 3D SLDV requires perfect steady-state conditions of the structure, which is not realistic in a time-consuming full-field measurement [19]. Multiple reasons such as room heating, minor

changes of the structural dynamics and even round errors of the system may contribute to the spatial inconsistency of measured data [19]. Further, in a nonlinear structural test setting, the phase lag between the measured acceleration and the input force is frequently taken as a control target (also known as nonlinear phase resonance testing [5,20-23]). It allows slight fluctuations of the driving frequency during a full-field measurement and thus adds new contributing factors to the inconsistency of datasets. This spatial inconsistency problem has to be resolved in order to use a 3D SLDV in a full-field nonlinear modal test.

One effective way to mitigate the spectral leakage effects for a multi-frequency signal is to resort to interpolation algorithms. Jain *et al.* [14] were the first to introduce an interpolation algorithm for the harmonic analysis of a multi-frequency signal and named it interpolated FFT algorithm. In the pioneering work, analytical expressions of the rectangular window were used to compensate for the short-range leakage of the signal spectrum, and a high accuracy measurement of the amplitudes and phases of the constituent sinusoids was achieved. Later, Grandke [15] proposed a method that can combine the merits of the tapered window algorithm and the interpolation algorithm, in which the former suppresses the long-range leakages of the spectra and the latter counters the short-range leakages. More specifically, an interpolation formula for the spectrum of a multi-frequency signal tapered with a Hanning window was derived. Zhang *et al.* [17] further extended the interpolated FFT method by considering that the signal was tapered with a family of cosine-sum windows and derived the interpolation formulas for several window functions of the family. Recently, Duda [24] derived interpolation algorithms for non-cosine windows with narrow main lobes such as Kaiser-Bessel and Dolph-Chebyshev windows, which are believed to have better noise immunity. The abovementioned research works use simulated examples to show that the interpolated FFT method is effective for harmonic analysis of multi-frequency signals and achieved a high degree of accuracy. However, its performance to deal with real measurement data featuring short sampling intervals and various signal-to-noise (SNR) ratios still demand a thorough investigation. In this paper, our solution to reduce the spectral leakage effects of 3D SLDV spectrum is closely related to the interpolated FFT algorithm. The difference is that we consider interpolating signal sets that are harmonically related to each other instead of a single signal.

This paper aims to utilise the advantages of 3D SLDV, such as its wide frequency range, fine measurement resolution, and superior capability in dealing with complex geometries to measure full-field, multi-harmonic responses of a nonlinear structure vibrating at its resonance. The long measurement duration of a 3D SLDV is significantly reduced by using a super-short sampling interval for each scan point. A novel Multi-step Interpolated Fast Fourier Transform procedure is proposed to suppress the resulting spectral leakage and mitigate spatial inconsistency of 3D SLDV datasets attributed to minor fluctuations of the driving frequency. In the procedure, the instantaneous driving frequency is first interpolated using the force signal. In the following step, the interpolated frequency is used to perform a fixed-frequency interpolation for each harmonic of the response signals. Numerical validations are carried out to investigate the accuracy and robustness of the proposed procedure with regard to different signal frequencies and noise levels before it is applied to experimental data of an industrial-scale fan blade.

The following paper is organised as follows. In Section 2, the theoretical framework of the Multi-step Interpolated-FFT procedure is derived. Discussions on its accuracy and robustness through numerical examples are elaborated in Section 3. Section 4 presents its application on experimental data of a large-scale fan blade. Finally, conclusions and future perspectives are drawn in Section 5.

2. Theory

2.1. General equation

This paper considers the vibrations of light-weighted nonlinear structures governed by:

$$\mathbf{M}\ddot{\boldsymbol{u}} + \mathbf{C}\dot{\boldsymbol{u}} + \mathbf{K}\boldsymbol{u} + \boldsymbol{f}_{nl}\left(\boldsymbol{u}, \dot{\boldsymbol{u}}\right) = \boldsymbol{p}(t) \tag{1}$$

where $\mathbf{M}$, $\mathbf{C}$, $\mathbf{K}$ denote the mass, damping and stiffness matrices, respectively. $\ddot{\boldsymbol{u}}$, $\dot{\boldsymbol{u}}$ and $\boldsymbol{u}$ represent the acceleration, velocity and displacement vectors, respectively. Vector $\boldsymbol{f}_{nl}\left(\boldsymbol{u}, \dot{\boldsymbol{u}}\right)$ is the nonlinear restoring force, and vector $\boldsymbol{p}(t)$ is the external excitation applied to the structure during testing.

In this paper, the nonlinear phase resonance testing [5, 20-23] is carried out via a MISO vibration controller, leading to a single point, mono-harmonic force [5, 20-23] applied on the structure:

$$p(t)=A_p \cos\left(2\pi f_p t+\varphi_p\right), \tag{2}$$

where A_p, f_p and φ_p denote the magnitude, driving frequency and phase of the force, respectively.

With such a nonlinear phase resonance test setting, the structure will be vibrating at one of its resonance. It is assumed that the responses of the test structure are periodic and contain multiple harmonics. Herein, a 3D SLDV is used for the full-field measurement, such that the vibration of a scan point can be expressed as:

$$u_{(dir)}=\sum_{m=1}^{N_\kappa} A_m^{(dir)} \cos\left(2\pi m f_p t+\varphi_m^{(dir)}\right), \tag{3}$$

where $u_{(dir)}$ denote the responses in *x*, *y* and *z* directions for a scan point when $dir \triangleq x, y$ and z, respectively. N_κ represents the number of constituent harmonics that appeared in the responses. $A_m^{(dir)}$ and $\varphi_m^{(dir)}$ are the amplitude and phase of the m^{th} harmonic component, respectively.

Figure 1 illustrates simulated signal sets in a full-field phase resonance testing, highlighting signal lengths in the Multiple-Input-Single-Output (MISO) vibration controller and 3D SLDV. At the lower part of the figure, it is shown that the MISO vibration controller uses force appropriation algorithms [5, 20-23] to maintain the test structure vibrating at one of its resonances for the entire duration of 3D SLDV measurement. To do this, the vibration controller measures a single-point acceleration of the structure (usually a point with the maximal magnitude of the response) and the driving force for a relatively long duration and uses their phase lags in the feedback algorithm to adjust the frequency and magnitude of the input force. It is shown in the upper part of the figure that a 3D SLDV is used to measure the driving force and full-field responses of the structure simultaneously. A super-short duration (e.g. several cycles of vibration) is used for each scan point to reduce testing time. To deal with the spatial inconsistency of the datasets, two estimates of the driving force are now defined: i) the estimated values provided by the MISO vibration controller are called *average estimates*, in which a much longer sampling interval is used in the calculation. ii) the values obtained using 3D SLDV scan point datasets are *instantaneous estimates*, whose sampling interval is much shorter than the MISO vibration

controller. Note that the average estimates and the instantaneous estimates of the driving force should only have minor discrepancies in a successful test.

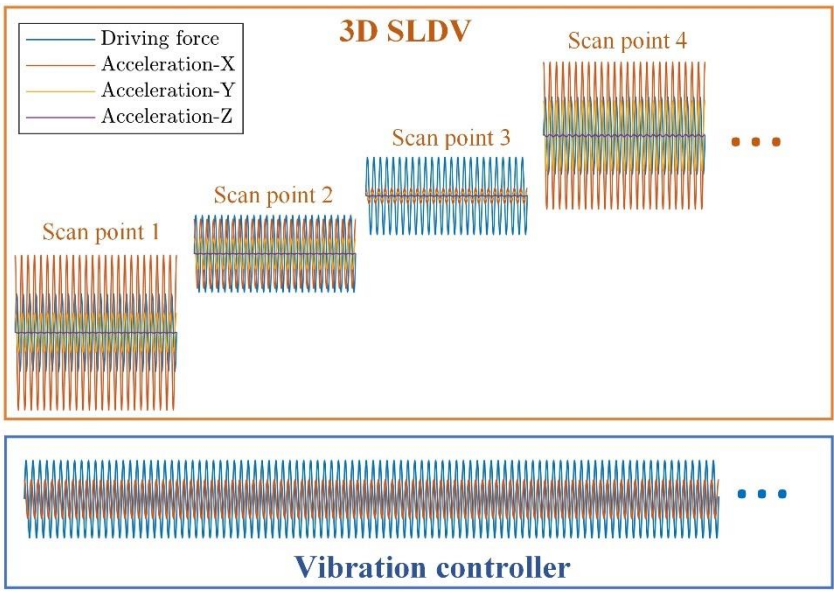

Figure 1. Illustration of signals sampled during a full-field measurement. The driving force signal is sampled by two systems: a MISO vibration controller and a 3D SLDV. A single-point acceleration is measured by the former, and full-field accelerations are measured by the latter.

Denoting the sampling rate of the 3D SLDV as $f^{\mathrm{SLDV}}=1/\Delta t$ and the acquisition time interval for each scan point as $T=N\Delta t$, four sequences of signals are sampled for each scan point:

$$p\left(k\Delta t\right)=A_p\cos\left(2\pi f_p\Delta t+\varphi_p\right),\quad k=0,1\cdots,N-1, \tag{4}$$

$$u_{(dir)}\left(k\Delta t\right)=\sum_{m=1}^{N_K}A_m^{(dir)}\cos\left(2\pi mf_p\Delta t+\varphi_m^{(dir)}\right),\quad k=0,1\cdots,N-1, \tag{5}$$

where $u_{(dir)}\left(k\Delta t\right)$ indicates x, y and z directional response when $dir\triangleq x,y$ and z, respectively. In the following derivations, the signals in each direction $u_{(dir)}$ are processed in the same way for a scan point. As such, the subscript $\bullet_{(dir)}$ is omitted for the sake of brevity.

It is also assumed that the sampling rate of 3D SLDV (f^{SLDV}) should well exceed the Nyquist rate of the highest constituent harmonics of the response signal to avoid aliasing errors. A common practice is to apply an anti-aliasing filter to the signal to limit its high-frequency content; thus, it requires [25]:

$$f^{\mathrm{SLDV}} > 2.56 \cdot N_{\kappa} f_p, \tag{6}$$

where 2.56 is the guard band ratio in accord with the anti-aliasing filter [26]. Note that a 3D SLDV can easily meet the requirement of Eq.(6) due to its wide-frequency measurement capability [7].

The discrete Fourier transform (DFT) of the force and response signals denoted by Eq. (4) and (5) are found to be:

$$P(n) = \frac{A_p}{2}\left[e^{\mathrm{j}\varphi_p} D\left(n - f_p/\Delta f\right) + e^{-\mathrm{j}\varphi_p} D\left(n + f_p/\Delta f\right)\right], \tag{7}$$

$$U(n) = \sum_{m=1}^{N_{\kappa}} \frac{A_m}{2}\left[e^{\mathrm{j}\varphi_m} D\left(n - mf_p/\Delta f\right) + e^{-\mathrm{j}\varphi_m} D\left(n + mf_p/\Delta f\right)\right], \tag{8}$$

where $U(n)$ represents one directional response of a scan point, n denotes the number of spectral line, $\Delta f = 1/T_m$ is the frequency resolution [4], $\mathrm{j}=\sqrt{-1}$ is the imaginary unit, and $D(\theta)$ denotes the Dirichlet kernel defined by:

$$D(\theta) = e^{-\mathrm{j}\pi\theta\left[(N-1)/N\right]} \frac{\sin(\pi\theta)}{N\sin(\pi\theta/N)}. \tag{9}$$

2.2. Challenges in signal processing of full-field data

In this paper, the full-field measurement for an industrial-scale structure targets as many as thousands of scan points. Consequently, a super short sampling interval for each scan point has to be chosen to achieve a reasonable testing time. It leads to a few challenges, particularly when measurements of nonlinear dynamic responses are required:

1) The first challenge is commonly called the 'grid effect' featured by a coarse frequency resolution of the DFT spectrum due to a finite length of the signal. For example, if $T_m \le 0.4$ s is set for each scan point, the frequency resolution of the response spectrum would be $\Delta f = 1/T_m \ge 2.5$ Hz, which is too coarse to meet the strict requirements in the aerospace industry and also has a high risk of not being able to describe the hardening or softening effects of a nonlinear mode.

2) The second challenge is the well-known 'spectral leakage' effect caused by non-coherent sampling. A coherent sampling requires an integer number of the vibrational signal period to be sampled, which is not practical for a 3D SLDV since its acquisition time is usually a fixed value and needs to be predefined before the measurement. In most cases, the 'true' frequency of the signal would not coincide with the DFT grid; thus, spectral leakage always occurs. Figure 2 illustrates the effects of spectral leakage with the aid of an example. A 51 Hz sinusoidal signal is sampled with a rate of

1024 Hz and an acquisition time interval of T_m=0.4 s, leading to a frequency resolution of Δf=2.5 Hz. It is clearly shown that the 'true' spectrum of the signal, which ideally should be a single sharp line at 51 Hz, leaks its energy to the sidelobes and results in a DFT spectrum (denoted by asterisks markers) that spilled over the entire frequency axis in the shape of the applied window function (marked by a solid black line).

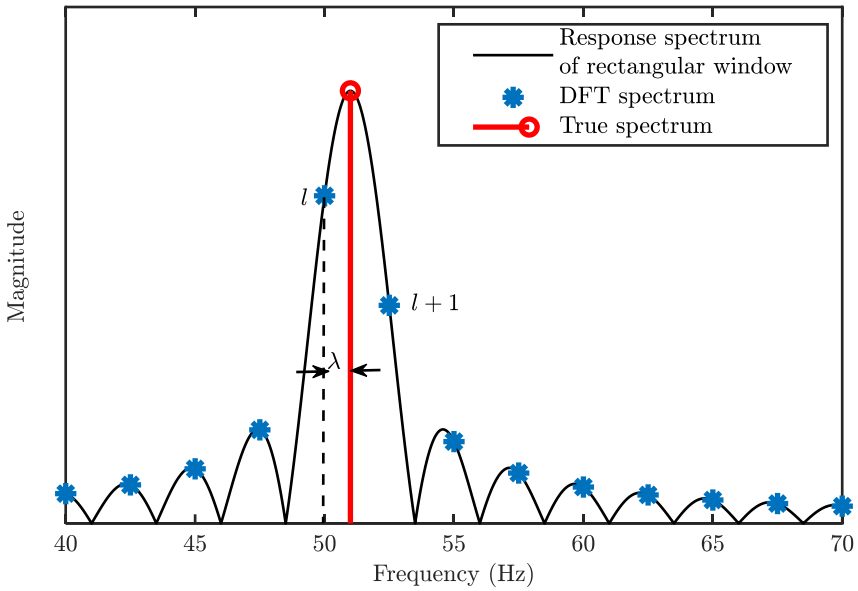

Figure 2. Example of grid effect and spectral leakage of the DFT spectrum, where a 51 Hz sinusoidal signal is sampled with a duration of T_m=0.4 s (Δf=2.5 Hz). The points denoted by l and l+1 represent the two adjacent points of the DFT spectrum in the vicinity of the 'true' peak and $\lambda \in [0,1)$ denote the distance between the point l and the 'true' line.

3) The third challenge is attributed to the multiple harmonics that exist in the dynamic response of a nonlinear structure. A conventional DFT for such a multi-harmonic signal would result in poor estimates of frequencies and amplitudes of the harmonics in the presence of spectral leakage. Tapering the signal with a smoothing window (e.g. a Hanning window) can minimise the long-range spectral leakage. However, the short-range leakage still exists. Moreover, the phase estimates for higher-order harmonics are generally believed to be erroneous [14-18], which will be further discussed using numerical examples in the next section.

4) The fourth challenge is associated with the spatial inconsistency of a full-field measurement using 3D SLDV [27]. As mentioned earlier, this issue becomes more evident in a nonlinear phase resonance test since phase lag is frequently

used as a control target [5,20-23] in such tests. Consequently, this minor frequency shift of the driving frequency significantly deteriorates the consistency of the measured dataset.

2.3. Multi-step Interpolated-FFT procedure

In this subsection, a novel Multi-step Interpolated-FFT procedure is proposed to resolve all the abovementioned challenges. Figure 3 depicts a flowchart illustrating the steps applied to the dataset of each scan point. Three major steps are highlighted:

1) Step A starts with the standard practice of applying a general window to the force and response signals to smooth the edges and remove the long-range spectral leakages [15]. Further treatments of the force and response signals are separated into two steps to enhance the robustness of the procedure.

2) In Step B, interpolation is applied to the force spectrum to provide instantaneous estimates of its fundamental harmonic component, i.e. instantaneous driving frequency, magnitude and phase. The accuracy of the interpolation process in Step B is validated by comparing the instantaneous estimates of the driving force to its average estimates provided by the MISO vibration controller, where a much longer sampling interval is used (see Figure 1).

3) Finally, the instantaneous driving frequency obtained in Step B is further used in Step C to perform a fixed-frequency interpolation for the response spectra in three directions and extract the parameters of the multi-harmonic responses of the same scan point.

Note again that the proposed procedure should be applied to the dataset of every scan point to obtain full-field results. The detailed equations are derived as follows:

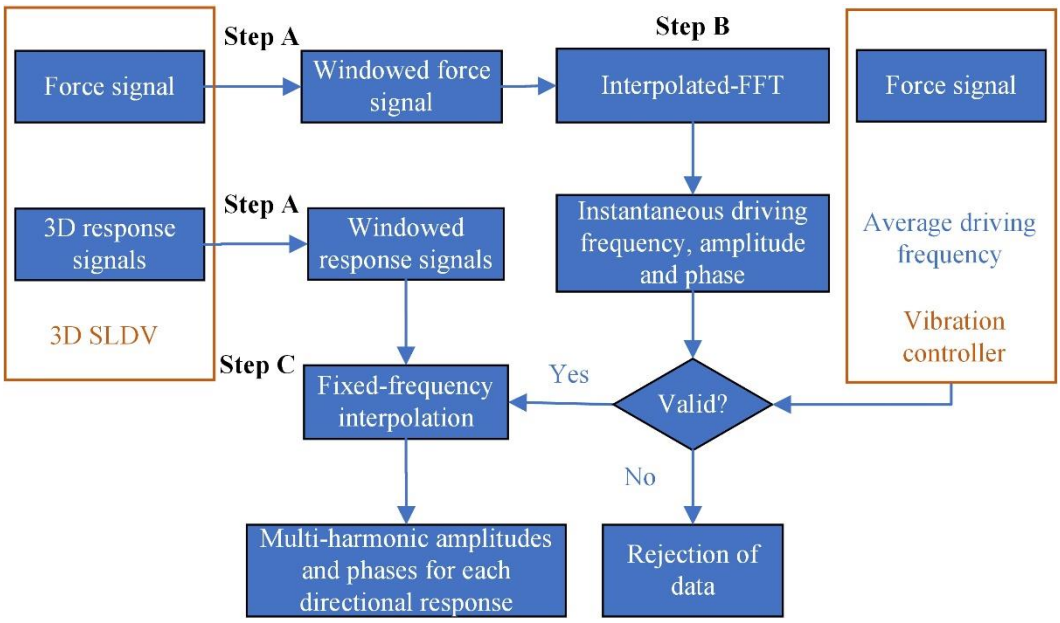

Figure 3. Illustration of the proposed Multi-step Interpolated-FFT procedure applied to the dataset of each scan point.

2.2.1. Step A. Long-range leakage reduction

As shown in Figure 3, the super-short sampled signals from the 3D SLDV are first tapered with a suitable window to smooth the edges and reduce the energy of the long-range leakage. No special requirement for the window is strictly needed, but a smoothing window with low sidelobe peaks can effectively remove the long-range leakage while maintaining a proper frequency resolution [17]. Then, without loss of generality, this paper considers tapering each of the N-point sampled signals with a cosine-sum window, whose general time-domain expression can be written as [17]:

$$w_{N_\tau}(k\Delta t)=\sum_{\tau=0}^{N_\tau}(-1)^{\tau}\,\alpha_\tau\cos\left(\frac{2\pi}{N}\tau k\,\Delta t/T\right),\quad k=0,1,\cdots,N-1, \tag{10}$$

where $N_\tau+1$ denotes the number of terms of the window and $\alpha_\tau\left(\tau=0,\cdots N_\tau\right)$ denotes the coefficients of the window. One can easily construct a commonly used window from the cosine-sum window family by substituting the coefficients into Eq. (10). For example, the coefficients of three windows considered in this paper - rectangular window, Hanning window and 4-term Blackman-Harris window [18] - are listed in Table 1.

Table 1. A list of windows and their corresponding window coefficients [18]

N_τ	Name of the window	Window coefficients

N_τ=0	Rectangular window	α_0=1
N_τ=1	Hanning window	α_0=α_1=1
N_τ=3	4-term Blackman-Harris window	α_0=0.35875,α_1=0.48829, α_2=0.14128,α_3=0.01168;

Figure 4 compares the windows' response spectra, where the peak sidelobe is -13 dB for the rectangular window, -31.5 dB for the Hanning window and only -92 dB for the 4-term Blackman-Harris window. It indicates that the 4-term Blackman-Harris window is more effective in attenuating the long-range leakage by using more terms to suppress the sidelobes, but the window has a much wider main lobe and a lower frequency resolution. In practice, a compromise has to be made between the long-range leakage reduction performance and the frequency resolution requirement, depending on the signal quality of the test results. It is very straightforward to find out that the proposed Multi-step Interpolated-FFT procedure can incorporate with any of the abovementioned windows as the general expression of the cosine-sum window family - Eq. (10) - is used in the derivations.

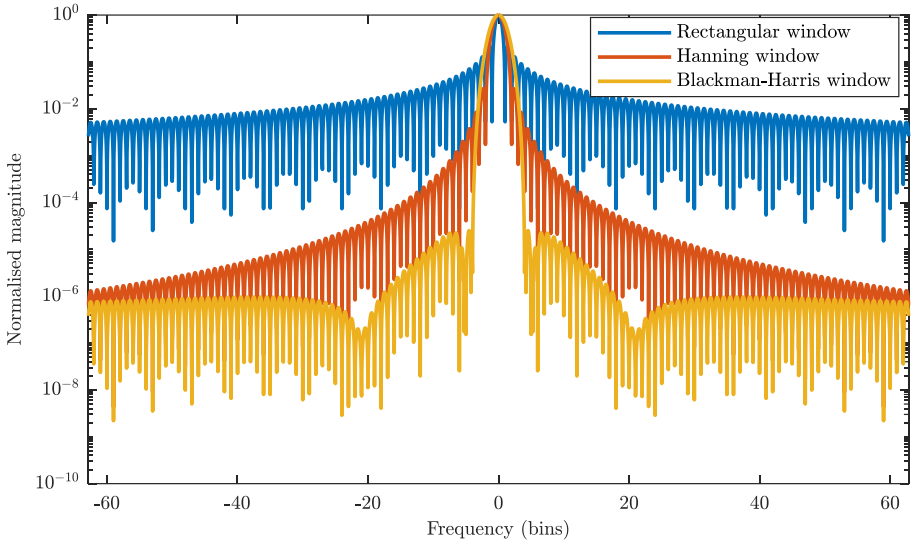

Figure 4. Comparison of response spectra of a rectangular window, a Hanning window and a 4-term Blackman-Harris window.

The tapered-window signal is a product of the sampled signal and the window function, i.e.,

$$\bar{p}(k\Delta t)=p(k\Delta t)\cdot w(k\Delta t), \tag{11}$$

$$\bar{u}(k\Delta t)=u(k\Delta t)\cdot w(k\Delta t). \tag{12}$$

It is assumed that the chosen window can effectively suppress the long-range leakage from the negative spectrum or other harmonic components of the signal. Consequently, the DFT spectrum of the tapered-window signal, which is the convolution of the signal spectrum and the window spectrum, can be simplified to [14-16]:

$$\bar{P}(n) \approx \frac{A_p}{2} e^{\mathrm{j}\varphi_p} W\left(n - f_p/\Delta f\right), \tag{13}$$

$$\bar{U}_m(n) \approx \frac{A_m}{2} e^{\mathrm{j}\varphi_p} W\left(n - m f_p/\Delta f\right), \quad m = 1, 2, \cdots N_\kappa, \tag{14}$$

where $\bar{P}(n)$ is the fundamental harmonic of the tapered-window force signal. $\bar{U}_m(n)$ is the m^{th} harmonic component of the tapered-window response signal $\bar{U}(n)$ and $W(\theta)$ is the Fourier transform of the chosen window. One attractive property of the cosine-sum window is that $W(\theta)$ can be analytically expressed as an algebraic sum of the Dirichlet kernels [17]:

$$W(\theta) = \sum_{\tau=0}^{N_\tau} (-1)^\tau \frac{\alpha_\tau}{2} \left[D(\theta - \tau) + D(\theta + \tau) \right]. \tag{15}$$

It can be seen from Eqs. (13) and (14) that the so-called short-range leakage [15] exists in the tapered-window spectrum if the coherent sampling condition is not satisfied, i.e. $W\left(n - f_p/\Delta f\right) \neq 1$ if $f_p/\Delta f$ is not an integer. As a result, only a moderate accuracy is achieved for the amplitude and frequency estimates of the harmonics, while the phase estimates for higher-order harmonics are generally believed to be erroneous [15-17].

2.2.2. Step B. Interpolate force spectrum

An interpolation algorithm [14-17] is then applied to the tapered-window spectrum of the driving force signal to counter the short-range leakage. In nonlinear phase resonance testing, the driving force signal should have a very high SNR, and ideally, it is supposed to be a mono-harmonic signal. Therefore, one would expect its 'true' spectral line, f_p, to exist somewhere between the largest two spectral lines in the tapered-window spectrum.

As shown in Figure 2, let l_p and $(l_p + 1)$ be the number of the largest two lines respectively, where l_p is an integer, and denote the interpolate distance λ_p as the 'true' location of the peak, i.e.,

$$f_p = \left(l_p + \lambda_p\right)\Delta f, \quad \text{with} \quad \lambda_p \in [0, 1). \tag{16}$$

Substituting Eq. (16) into Eq. (13), one would obtain the spectrum of the tapered-window force signal in the form of:

$$\bar{P}(n)=\frac{A_p e^{j\varphi_p}}{2}W\left(n-l_p-\lambda_p\right), \tag{17}$$

where n is the spectral line. Eq. (17) shows that the spectrum contains a $W\left(n-l_p-\lambda_p\right)$ profile of the window. If a non-integral number of signal cycles are sampled, the window function smears a single sinusoid onto the entire spectrum, where the adjacent lines around the peak - l_p and $\left(l_p+1\right)$ - are profoundly affected by the short-range leakage. To reduce its effects, an analytical expression of the ratio of the two magnitudes of the adjacent lines [14] is used, which reads:

$$\eta_p=\frac{\left|\bar{P}\left(l_p+1\right)\right|}{\left|\bar{P}\left(l_p\right)\right|}=\left|\frac{W\left(1-\lambda_p\right)}{W\left(-\lambda_p\right)}\right|=\mathcal{F}\left(\lambda_p\right). \tag{18}$$

It is shown by Eq.(18) that the ratio (η_p) is determined by the distance of the interpolated point λ_p and the tapered window function [14-17]. Analytical approximations of $\mathcal{F}(\bullet)$ for specific windows such as a rectangular window (Jain et al. [14]), a Hanning window (Grandke [15]), and a 4-term Blackman Harris window (Zhang [17]) have already been derived in the literature. Here, a more general form for the approximation of $\mathcal{F}(\bullet)$ is presented to allow full generalisation of the method.

Consider the number of sampled points (N) to be a large number, such that the following approximation holds [17]:

$$\sin\left(\pi\left(-\lambda_p+\tau\right)/N\right)\approx\pi\left(-\lambda_p+\tau\right)/N. \tag{19}$$

Assuming τ as an integer, and substituting Eq. (19) into the Dirichlet kernel of Eq. (9) leads to

$$\begin{aligned} D\left(-\lambda_p+\tau\right) &= e^{-j\pi\left(-\lambda_p+\tau\right)\left[(N-1)/N\right]}\frac{\sin\left(\pi\left(-\lambda_p+\tau\right)\right)}{N\sin\left(\pi\left(-\lambda_p+\tau\right)/N\right)} \\ &\approx e^{j\pi\lambda_p}\frac{\sin\left(\pi\lambda_p\right)}{\pi\left(\lambda_p-\tau\right)}, \end{aligned} \tag{20}$$

Substituting Eq. (15) into Eq. (18) and using the approximation of Eq. (20), Eq. (18) can be rewritten as:

$$\mathcal{F}\equiv\left|\sum_{\tau=0}^{N_\tau}\frac{(-1)^\tau\alpha_\tau\left(\lambda_p-1\right)}{\left(\lambda_p-\tau-1\right)\left(\lambda_p+\tau-1\right)}\right|\Bigg/\left|\sum_{\tau=0}^{N_\tau}\frac{(-1)^\tau\alpha_\tau\lambda_p}{\left(\lambda_p-\tau\right)\left(\lambda_p+\tau\right)}\right|. \tag{21}$$

Eq. (21) is a general expression for the family of cosine-sum windows. One can then get the expression of $\mathcal{F}(\bullet)$ for a specific window by substituting the corresponding window coefficients into Eq. (21).

Figure 5 illustrates the shape of $\mathcal{F}(\bullet)$ a rectangular window, a Hanning window, and a 4-term Blackman-Harris window. It can be seen that the slope of $\mathcal{F}(\bullet)$ is smaller for a 4-term Blackman-Harris window compared to the other two windows, which indicates that the window's ratio of magnitudes is less sensitive to the interpolation distance λ_p. It is also apparent that the $\mathcal{F}(\bullet)$-functions intersect at one point (0.5,1) due to symmetrical response spectra of the considered windows [18].

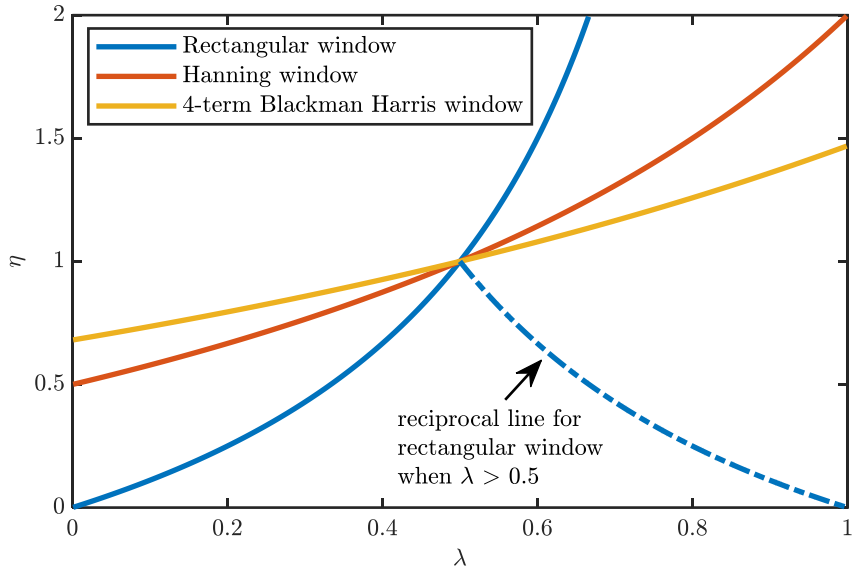

Figure 5. The ratio of magnitudes for a rectangular window, a Hanning window and a 4-term Blackman-Harris window.

Here, the ratio of magnitudes $\mathcal{F}(\bullet)$ is used inversely in the interpolation algorithm [14-17] to infer the interpolation distance λ_p, i.e.

$$\lambda_p = \mathcal{F}^{-1}(\eta_p), \tag{22}$$

where the magnitude ratio - η_p - of the two largest adjacent lines is estimated from the tapered-window spectrum of the forcing signal, see Eq. (18). Herein, Eq. (22) is referred to as the *interpolation distance function*.

Substituting the coefficients from Table 1 into Eqs. (21) and (22) would lead to the individual expressions presented in Refs. [14,15,17]. Note that the interpolation distance function - $\mathcal{F}^{-1}(\bullet)$ - is ill-conditioned for a rectangular window

when $\lambda_p \to 1$, therefore, its reciprocal line must be used when $\lambda_p > 0.5$; For any other window with a wider main lobe, $\mathcal{F}^{-1}(\bullet)$ is well conditioned and requires no special treatment.

After obtaining the interpolation distance λ_p, the fundamental harmonic force can be estimated using the relative larger component (denoted as $\tilde{P}$) of the two adjacent lines [15-17]. Due to the symmetrical shape of the window spectrum, it is not difficult to find out that:

$$\tilde{P}=\begin{cases} \bar{P}(l_p) & \text{if} \quad 0 \le \lambda_p < 0.5, \\ \bar{P}(l_p+1) & \text{if} \quad 0.5 \le \lambda_p < 1. \end{cases} \tag{23}$$

Then the complex coefficient of the fundamental harmonic of the input force, $\bar{P}(l_p+\lambda_p)$, can be interpolated by

$$\bar{P}(l_p+\lambda_p)=\begin{cases} \tilde{P}/W(-\lambda_p) & \text{if} \quad 0 \le \lambda_p < 0.5. \\ \tilde{P}/W(1-\lambda_p) & \text{if} \quad 0.5 \le \lambda_p < 1, \end{cases} \tag{24}$$

Finally, the magnitude and the phase of the driving force signal can be deduced from the complex coefficient $\bar{P}(l_p+\lambda_p)$ using Eq. (13).

Note that the force signal is sampled by both systems (a MISO vibration controller and a 3D SLDV) simultaneously (see Figure 1). Therefore, the instantaneous driving frequency interpolated using signals of each scan point of 3D SLDV should not deviate too far from the average driving frequency provided by the MISO vibration controller. Otherwise, the data should be rejected for further analysis, as shown in Figure 3.

2.2.3. Step C. Interpolate response spectrum

The final step of the procedure is to apply a fixed-frequency interpolation for the windowed response spectra of the same scan point. The distance of interpolation for each harmonic at this step is directly calculated using the instantaneous frequency of the input force (obtained in Step B); this assumes that the sinusoids in the response signals are harmonically related to the input force during a phase resonance test. With this assumption, the distance of interpolation (λ_m) for the m^{th} harmonic component of the response signal can be expressed as:

$$\lambda_m = m f_p / \Delta f^{\text{SLDV}} - l_m \quad \text{with} \quad \lambda_m \in [0,1), \tag{25}$$

where l_m=floor$\left(mf_p/\Delta f^{\mathrm{SLDV}}\right)$, f_p denotes the instantaneous driving frequency estimated in Step B by using the input force signal of the same scan point.

Using the interpolation distances of Eq.(25), the parameters of the response signals of can be obtained analogously to Step B, i.e. getting a complex coefficient for each harmonic:

$$\bar{U}_m\left(l_m+\lambda_m\right)=\begin{cases}\tilde{U}_m/W\left(-\lambda_m\right) & \text{if} \quad 0\le\lambda_m<0.5,\\ \tilde{U}_m/W\left(1-\lambda_m\right) & \text{if} \quad 0.5\le\lambda_m<1.\end{cases} \tag{26}$$

where $\tilde{U}_m$ is the larger amplitude of the two adjacent lines $\bar{U}_m\left(l_m\right)$ and $\bar{U}_m\left(l_m+1\right)$, i.e.,

$$\tilde{U}_m=\begin{cases}\bar{U}_m\left(l_m\right) & \text{if} \quad 0\le\lambda_m<0.5,\\ \bar{U}_m\left(l_m+1\right) & \text{if} \quad 0.5\le\lambda_m<1.\end{cases} \tag{27}$$

Note again that the interpolation Step C needs to be carried out for each harmonic component and each scan point's directional response.

Finally, to obtain full-field operating deflection shapes, Steps A to C are performed for each scan point in a successive way.

3. Numerical examples

In this section, the proposed Multi-step Interpolated-FFT procedure is validated through numerical examples containing signal sets (input force and response signals) as would be expected by a single scan point measured using a 3D SLDV. Frequencies, amplitudes and phases of the signals are thereby randomly chosen. To reflect the features of signals from a typical nonlinear phase resonance test, each example includes:

1) A pair of simultaneously measured driving force and response signals, as denoted by Eqs. (4) and (5). The input force signal is a single sinusoid with a magnitude of 1 and a phase of 0; the response signal represents one directional response of a scan point. It is composed of 10 harmonic terms, in which the fundamental frequency is the same as the driving force. Without loss of generality, the amplitudes and phases of the response signal are randomly chosen in the interval of (1e-4,10) and (0, 360), respectively [28]. The sampling time intervals and values of the chosen fundamental frequencies are listed in Table 2.

2) Each signal is then polluted with additive, zero-mean, and uniformly distributed Gaussian noise [28] over an interval linked to the smallest magnitude of the constituent harmonic:

$$\left[-\sigma A_{\min},\ \ \sigma A_{\min}\right], \tag{28}$$

where σ denotes the reference noise level and $A_{\min}=\min\left(\mathrm{abs}\left(A_m\left(m=1,2,\cdots 10\right)\right)\right)$ denotes the magnitude of the weakest harmonic of the signal. Herein, a signal-to-noise ratio indicating whether a harmonic peak sufficiently 'stands out' from the noise floor is post-evaluated by:

$$SNR=10\log_{10}\frac{A_{\min}^2}{\max\left(A_{noise}\right)^2}, \tag{29}$$

where A_{noise} denotes the maximum spectral component of the noise floor. The reference noise level - σ - is taken as 0.5% for the input force signal while it varies for the response signals in each example, as specified in Table 2.

3) The sampling rate is considered as 12.5 kHz for all the examples, which well exceeds the Nyquist sampling rate for all the constituent harmonics of the simulated signals.

Table 2. Parameters of the simulated examples.

Parameters		First example	Second example	Third example
Harmonic analysis method	Tapered-window FFT method*	√	√	×
	Multi-step Interpolated-FFT procedure**	√	√	√
Sampling interval	Three intervals (16 s, 1.6 s and 0.16 s)	√	×	×
	Fixed at 0.16 s	√	√	√
Fundamental frequency	Increase from 200 Hz to 206.25 Hz with a step of 1.25 Hz	×	√	×
	Fixed at 203.33 Hz	√	×	√
Reference noise level of the response signal σ	Varies from 5% to 250%	×	×	√
	Fixed at 5%	√	√	×
Total number of random realisations of signal sets		1	30000	30000

*The signal is tapered with a 4-term Blackman-Harris window in the tapered-window FFT method in this section; therefore, the spectra of the tapered-window FFT method are adjusted by an amplitude correction factor of 2.7875 before comparing to the 'true' amplitudes [18].

**The 4-term Blackman-Harris window is also used in the Multi-step Interpolated-FFT method (Step A) in order to compare its performance with the conventional tapered-window FFT method.

To compare the accuracy of the proposed Multi-step Interpolated-FFT procedure and the conventional tapered-window FFT method, two types of errors are defined herein: (a) *relative amplitude error* as the value of the absolute amplitude error divided by the true amplitude and (b) *absolute phase error* as the discrepancy between the estimated phase and the true phase for each constituent harmonic of the signal, respectively. These errors are illustrated in detail for each harmonic component in the first example, whereas their root-mean-square (RMS) values are used in the second and the third examples:

$$RMS(\varepsilon) = \sqrt{\frac{1}{N_\kappa}\sum_{m=1}^{N_\kappa}\varepsilon_m^2}, \tag{30}$$

where ε_m denotes the error of m^{th} harmonic component.

3.1. First example: accuracy of interpolation

The first example is used to illustrate the superior accuracy of the proposed Multi-step Interpolated-FFT procedure by comparing its estimate errors with those obtained by using the conventional tapered-window FFT method. Only one signal set is used in this example, of which the randomly chosen amplitudes and phases of the response signal are listed in Table 3. It is worth noting that the input force and response signals are polluted by white noises with reference noise levels of 0.5% (*SNR* ~ 65 dB) and 5% (*SNR* ~ 45 dB), respectively. Other settings of this example have already been detailed in Table 2.

Table 3. Randomly chosen amplitudes and phases of the harmonics in the response signal.

Harmonic order	**1**	**2**	**3**	**4**	**5**	**6**	**7**	**8**	**9**	**10**
Amplitude	8.147	9.058	1.270	9.134	6.324	0.975	2.785	5.469	9.575	9.649
Phase (°)	56.741	349.41	344.58	174.74	288.1	51.079	151.83	329.66	285.19	345.42

Figure 6 depicts the time series of the signals where three sampling time intervals are considered to highlight the grid effect and spectral leakage of the spectrum. The scenarios of 1.6 s and 0.16 s are obtained by selecting the first 1.6 s and first 0.16 s of data from the 16 s dataset. As listed in Table 2, the fundamental frequency of the signals is taken as 203.33 Hz to ensure a non-integer number of cycles of the signals are sampled; therefore, spectral leakage always occurs for these three scenarios.

Firstly, the conventional tapered-window FFT method (with a 4-term Blackman-Harris window) is applied to the simulated input force signal, leading to the results summarised in Table 4. It is not surprising to find out that a longer sampling time interval generally yields a smaller frequency error since its maximum can only be $\Delta f/2$.

Secondly, the conventional tapered-window FFT method is applied to the response signals, leading to the spectra shown in Figure 7. A glance at Figure 7 (a) indicates that the gird effects would be marginal if a 16 s signal is used: the harmonic components would appear as sharp peaks in the spectrum with a fine frequency resolution of 0.0625 Hz. However, this measurement interval for each scan point (i.e. 8.89 hours for a full-field scan of some 2000 points) is not practical in a real test. If the sampling interval reduces to a preferable duration of 0.16 s, it is clearly shown in Figure 7(c) that the spectrum would have noticeable grid effects as the spectral lines are spaced with a step of 6.25 Hz. In addition to this, much wider peaks are also observed in the figure due to spectral leakages. Figure 8 illustrates the relative amplitude error and the absolute phase error of the response signal in terms of each harmonic component. It can be seen that an increase of sampling time does not necessarily improve the estimation accuracy of the harmonic amplitudes and phases even when a 4-term Blackman-Harris window is applied to the signals before DFT. A moderate accuracy of 10% in terms of relative amplitude error is achieved, and accurate phase estimates are only guaranteed for the fundamental harmonics. It is clearly shown in Figure 8 (b) that the phase estimates for higher-order harmonics are erroneous due to spectral leakages [14-18].

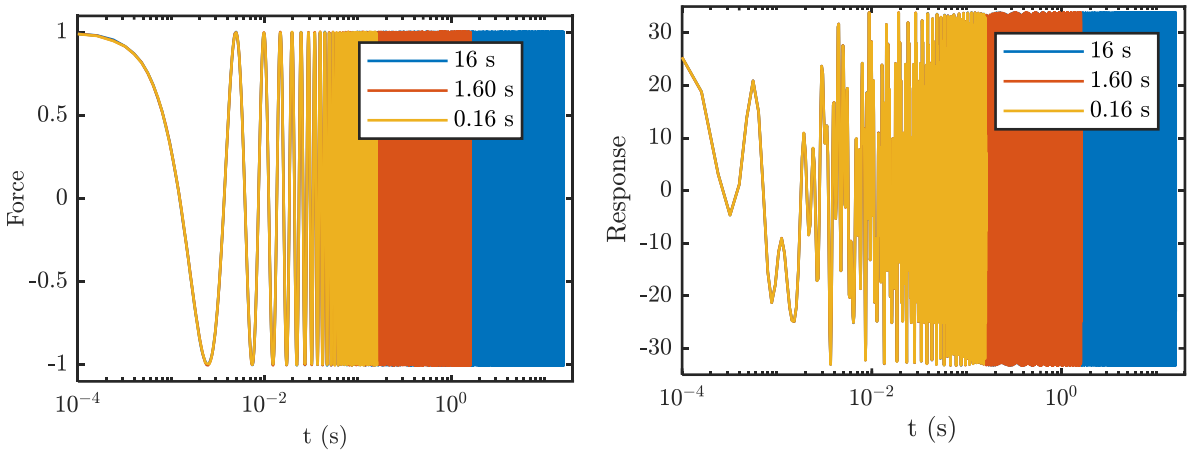

(a) (b)

Figure 6. Simulated vibration signals featuring three sampling intervals: (a) the input force signal and (b) the response signal.

Table 4. Frequency and amplitude estimates of the input force signal.

	Tapered-window FFT method applied to 16 s signal set	**Tapered-window FFT method applied to 1.6 s signal set**	**Tapered-window FFT method applied to 0.16 s signal set**	**Multi-step Interpolated-FFT procedure applied to 0.16 s signal set**
Estimated frequency (Hz)	203.3125	203.1250	206.2500	203.4309
Frequency error (Hz)	0.0175	0.2050	2.9200	0.1009
Estimated amplitude	0.9672	0.9560	0.9253	0.9997
Relative amplitude error	3.28%	4.4%	7.47%	0.03%

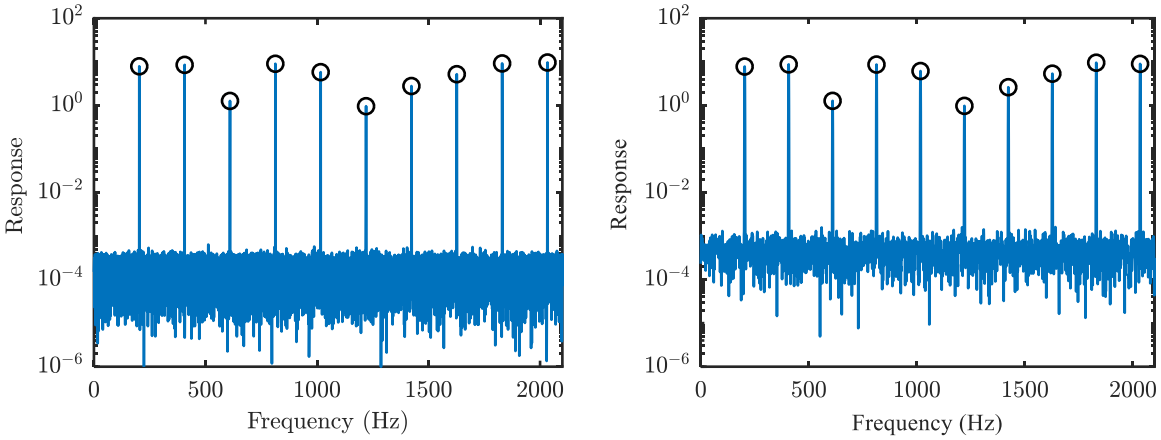

(a) (b)

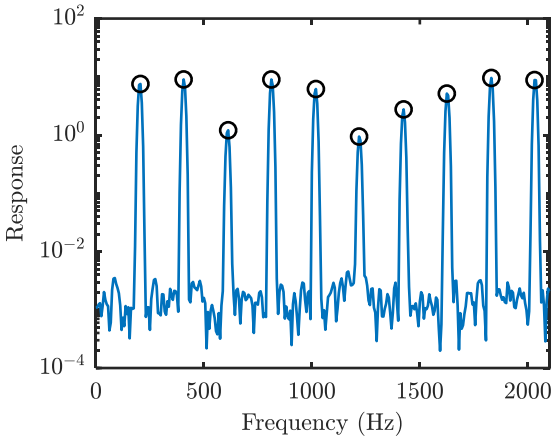

(c)

Figure 7. Tapered-window FFT spectra of the response signals featuring three sampling intervals: (a) 16 s, (b) 1.6 s and (c) 0.16 s.

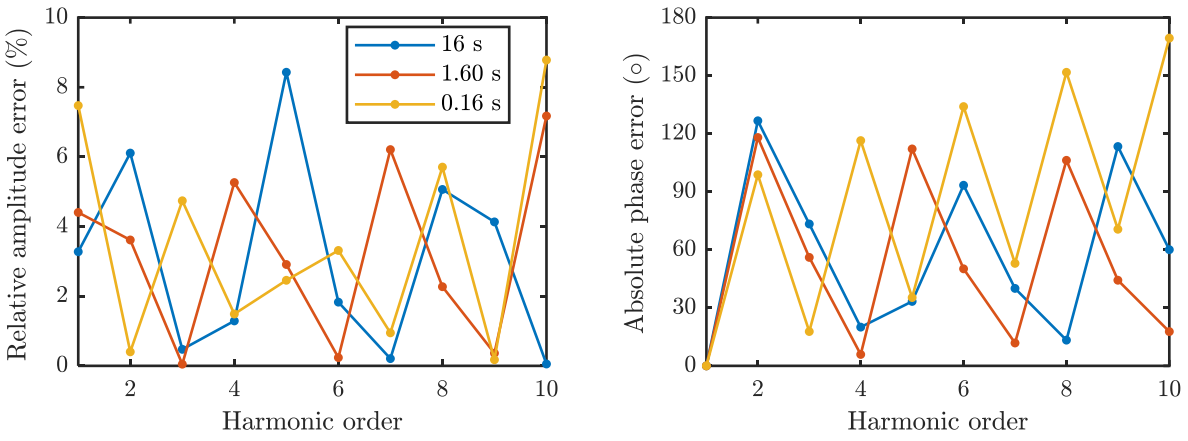

(a) (b)

Figure 8. The errors of the tapered-window FFT method applied to the response signals: (a) relative amplitude error and (b) absolute phase error.

Thirdly, the proposed Multi-step Interpolated-FFT procedure is applied to the shortest force signal of 0.16 s only, where a 4-term Blackman-Harris window is also used in the first step for comparison. Figure 9 illustrates the interpolated peak by applying the Multi-step Interpolated-FFT procedure, where the peak is seen between the two largest spectral lines of the tapered-window FFT spectrum of the force signal. Table 4 also compares its frequency and amplitude estimates to the results of the conventional tapered-window FFT method. It is shown that the proposed procedure achieves a frequency error of only 0.1 Hz by using the shortest 0.16 s signal, while the conventional tapered-window FFT method has to use a

1.6 s signal to reach a 0.2 Hz frequency error. If both methods were applied to the same length signal of 0.16 s, the proposed method provides an order of magnitude smaller error in terms of driving frequency estimate, as listed in Table 4. More importantly, the proposed method has achieved two orders of magnitude improvements in terms of the amplitude estimate for the driving force signal compared to the tapered-window FFT method applied to all three signal sets considered in this example.

Fourthly, the Multi-step Interpolated-FFT procedure is applied to the response signal of 0.16 s, as shown in Figure 10. A maximum of 0.14% error for the relative amplitude and a maximum of 0.2° of absolute phase error are observed for all harmonics, which are also orders of magnitudes better than the results from the tapered-window FFT method (see Figure 8). The comparisons made in this example highlight the proposed procedure's superior accuracy in estimating frequencies, amplitudes, and phases of multiple harmonics for super-short signals.

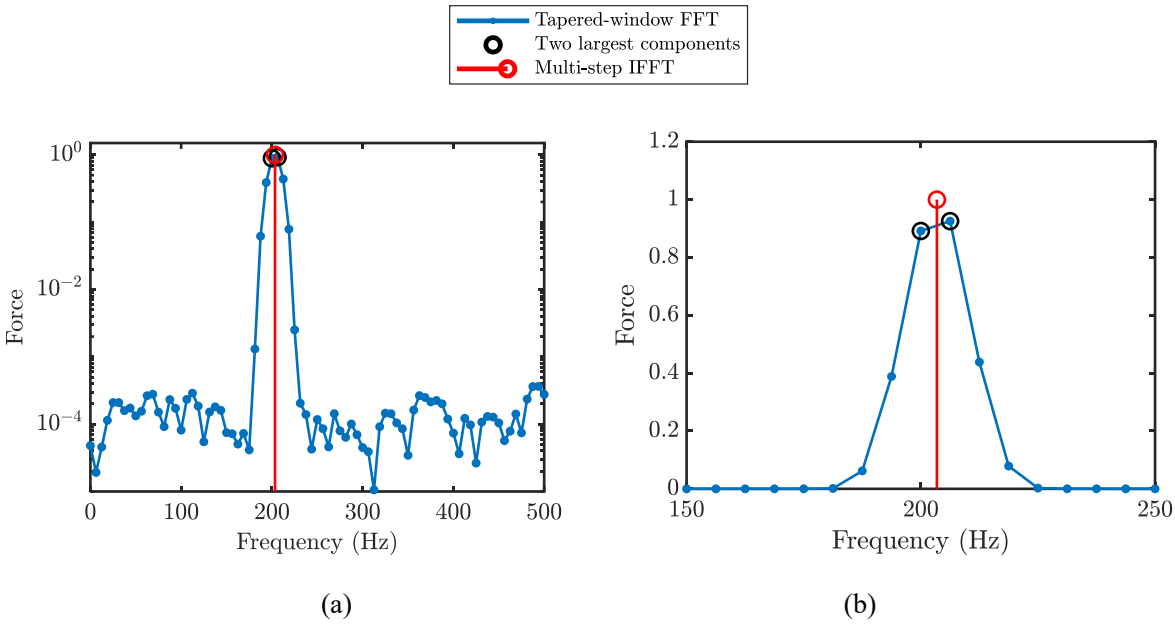

(a) (b)

Figure 9. Two largest adjacent lines and the interpolated peak of the input force signal: (a) logarithmic scale of the y-axis where the noises are visible and (b) zoomed-in view with a linear scale of the y-axis.

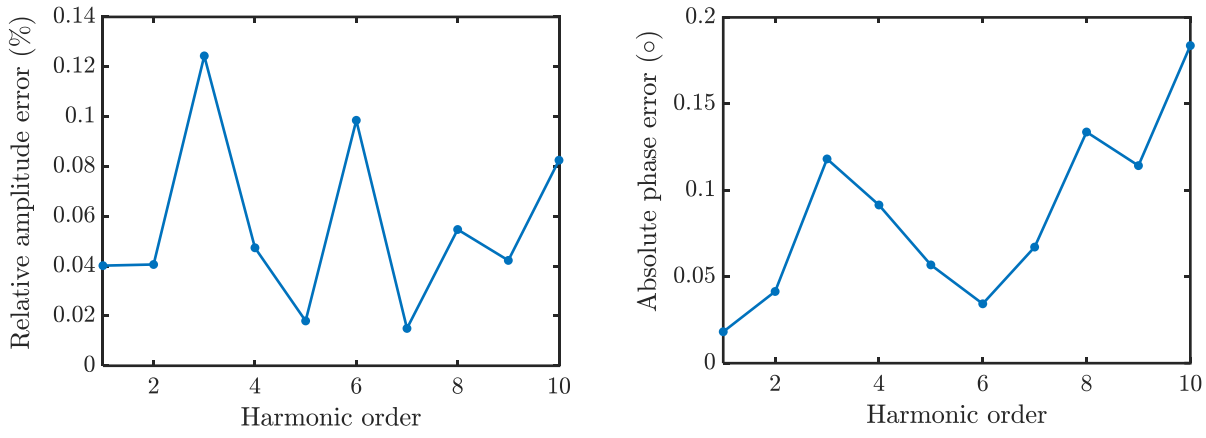

Figure 10. The errors of the Multi-step Interpolated-FFT procedure applied to the response signal of 0.16 s: (a) relative amplitude error and (b) absolute phase error.

3.2. Second example: the effect of signal frequency

It is known that the relation between the frequency of the signal and the frequency resolution (or equivalently, sampling time interval) would dictate the level of spectral leakage and thus affect the accuracy of harmonic analysis results. For example, the leakage would be minimal for the tapered-window FFT method if an integral number of cycles of the signal is sampled; otherwise, the accuracy would be heavily jeopardised, as seen in the first example. To ensure that the proposed Multi-step Interpolated-FFT procedure does not suffer from similar issues, its sensitivity with respect to the driving frequency (i.e. fundamental frequency of the sampled signals) must be evaluated. The second example focuses consequently on the targeted sampling time interval of 0.16 s while increasing the fundamental frequency of the input force from 200 Hz to 206.5 Hz with a step of 1.25 Hz; the frequencies of the harmonics in response signals are then adjusted accordingly. Without loss of generality, five thousand random realisations of different amplitudes and phases of the response signals are carried out at each frequency step to validate the proposed procedure, leading to a total of thirty thousand realisations of signal sets in this example. Note that the force and response signals are polluted by white noises with fixed levels of $\sigma = 0.5\%$ and $\sigma = 5\%$, respectively, for each signal set. Other detailed settings for this example are listed in Table 2.

Figure 11 and Figure 12 show the RMS values of the relative amplitude error and absolution phase error of the response signals calculated for each signal set, respectively. In each figure, the conventional tapered-window FFT method and the proposed Multi-step Interpolated-FFT procedure are compared. Not surprisingly, it can be seen from Figure 11(a) and Figure 12(a) that the tapered-window FFT method only achieves desired accuracy when the fundamental frequency of the signal is 200 Hz or 206.25 Hz, which are integral multiples of the frequency resolution (6.25 Hz). The relative amplitude error increases to the previously observed 7% for other frequencies, and the phase estimates for all the higher-order harmonics become very inaccurate. In contrast, the results of the Multi-step Interpolated-FFT method presented in Figure 11(b) and Figure 12(b) demonstrate consistent low levels of errors. Specifically, the RMS values of its relative amplitude errors are below 0.4%, and the RMS values of the absolute phase errors are no greater than 1° across all investigated driving frequencies. This is attributed to the multiple steps developed in the proposed procedure, in which the 'true' fundamental frequency is always interpolated in a first step by using the input force signal and then utilised to infer the amplitudes and phases of the constituent harmonics of the response signal in a subsequent step.

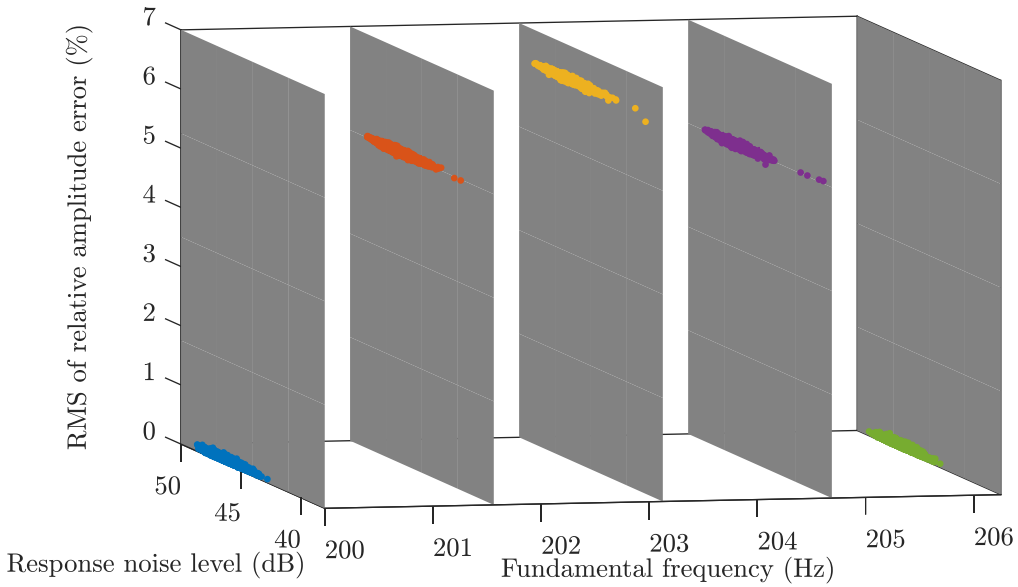

(a)

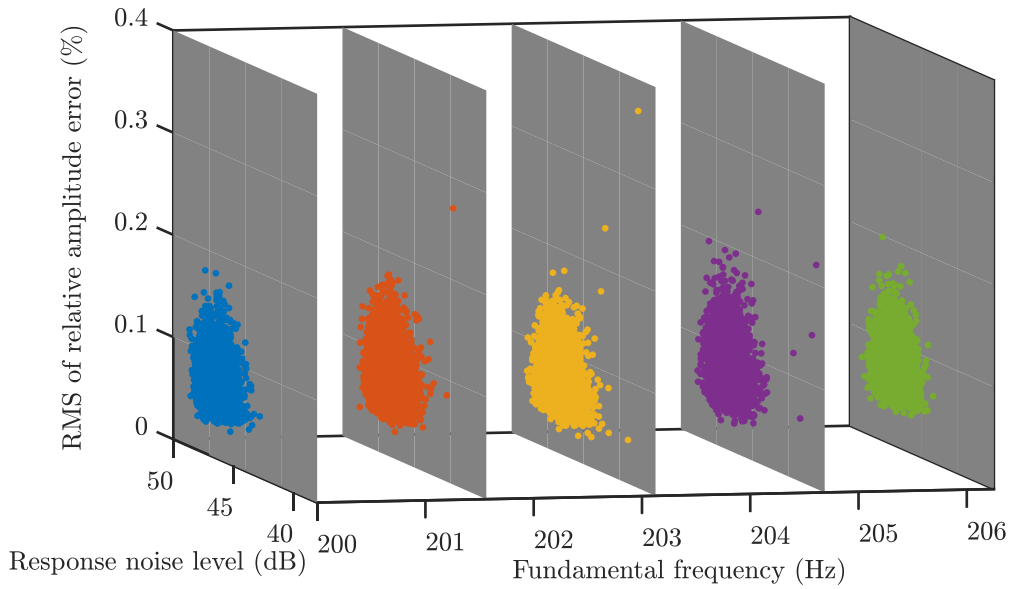

(b)

Figure 11. RMS values of the relative amplitude error by applying (a) the conventional tapered-window FFT method and (b) the proposed Multi-step Interpolated-FFT procedure to the signal sets.

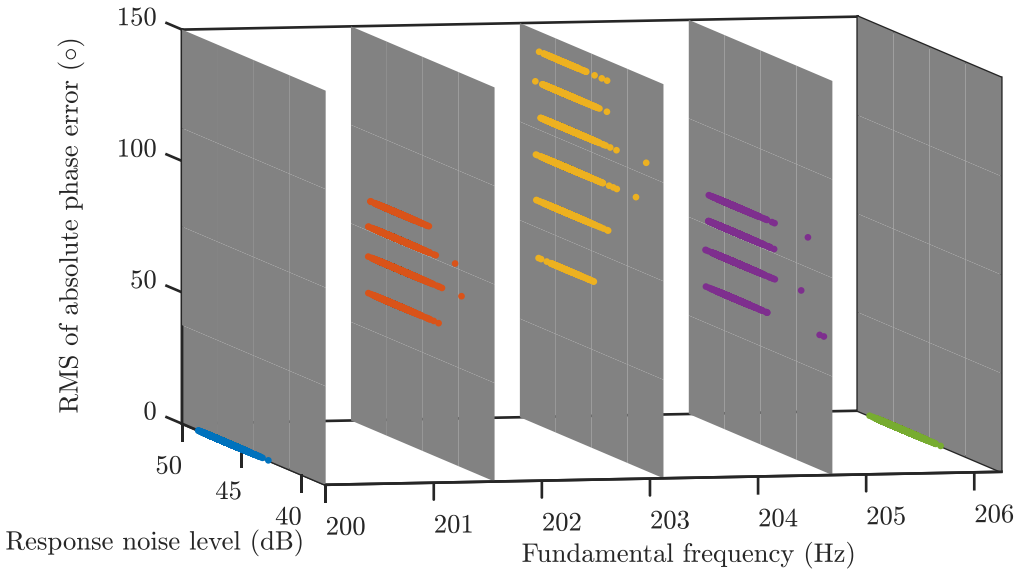

(a)

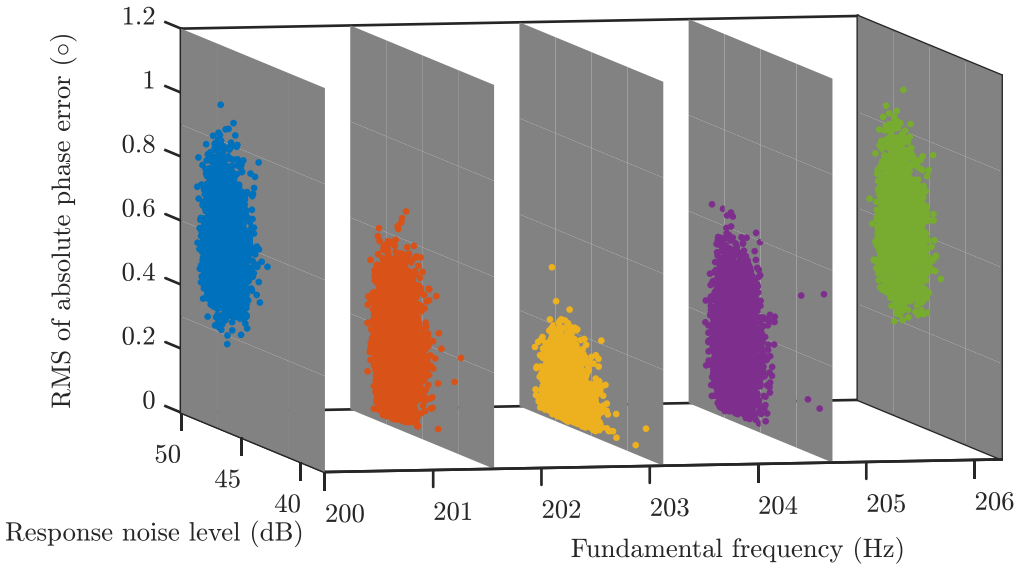

(b)

Figure 12. RMS values of the absolute phase error by applying (a) the conventional tapered-window FFT method and (b) the proposed Multi-step Interpolated-FFT procedure to the signal sets.

3.3. Third example: influence of noise level

Till now, the proposed Multi-step Interpolated-FFT procedure has been demonstrated reliable in the presence of a fixed level of noise in proceeding examples. In a realistic full-field test of a structure using 3D SLDV, the SNR of the input force signal can be quite large for each scan point since a steady-state, mono-harmonic excitation is used during the measurement. However, the SNRs of the response signals may vary significantly from point to point: they could be very low near nodal points and relatively high at anti-nodes. Also, the shape of the structure, contamination on the surface, and other environmental conditions can lead to substantial signal quality variations in the response measurement. To address this, the third example investigates the performance of the Multi-step Interpolated-FFT procedure in dealing with signal sets that have a fixed level of noise ($\sigma = 0.5\%$) in the input force signal but increases the noise level of σ from 5% to 250% for the response signals using six steps, as listed in Table 2. Again, five thousand random realisations of amplitudes and phases of the response signals are adopted at each step, leading to a total of thirty thousand realisations of signal sets.

Figure 13 and Figure 14 shows the RMS values of the relative amplitude and absolute phase errors versus the evaluated response SNRs, respectively. As can be seen, the Multi-step Interpolated-FFT procedure produces repeatable results for each noise level containing five thousand realisations of signal sets, indicated by clusters of point clouds with small distances to the centroid of the cluster. It can also be observed from Figure 13 that the maximum error of the proposed procedure increases with the level of noise. When the response SNRs are between 10 dB and 15 dB, the results show up to 9% relative amplitude error. If the SNR of the response signal reaches 35 dB, the relative amplitude errors become lower than 1%. The same trend applies to the absolute phase error shown in Figure 14, where the RMS values of all signal sets are below 6° if the response SNRs are between 10 dB and 15 dB and reduce to lower than 0.6° as response SNR reaches 35 dB. The results show that the proposed procedure is relatively robust against noise. When dealing with measured signals with multiple harmonics, an acceptable noise level for the response signals should be assessed for individual problems since it affects the target accuracy of the final results.

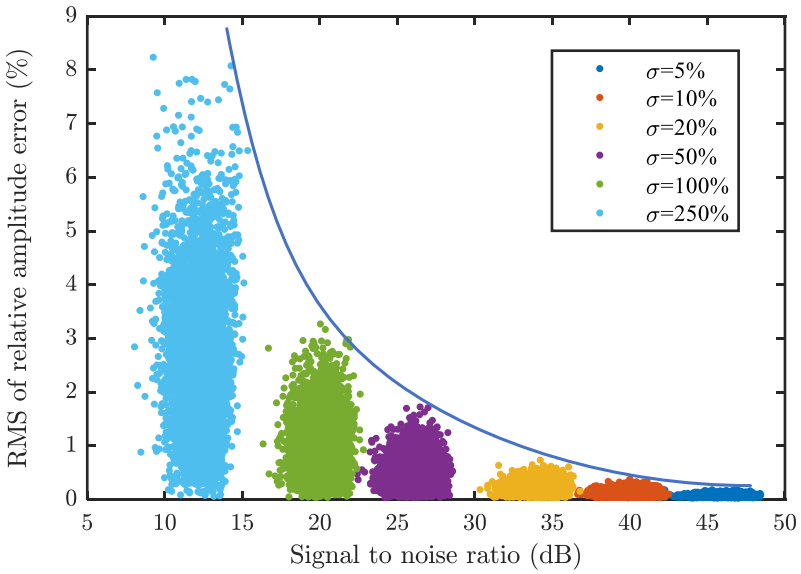

Figure 13. RMS values of the relative amplitude error versus SNR levels by applying the proposed Multi-step Interpolated-FFT procedure to the signal sets.

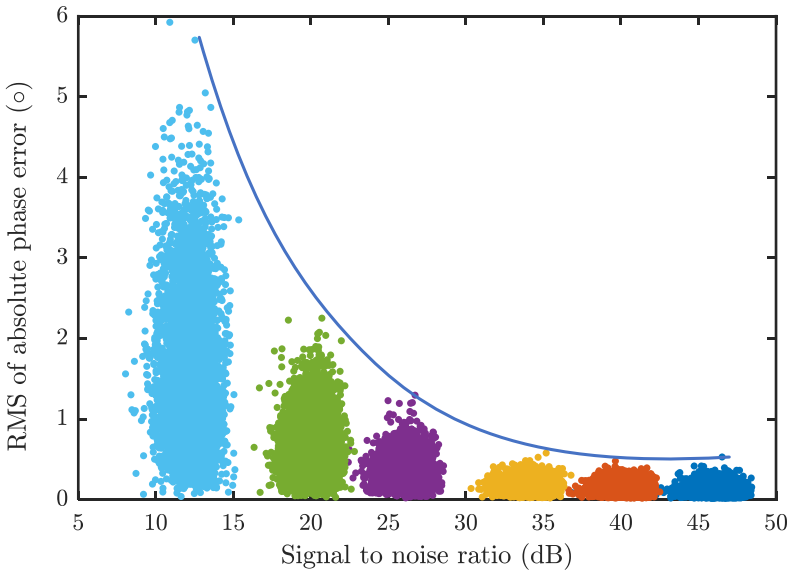

(b)

Figure 14. RMS values of the absolute phase error versus SNR levels by applying the proposed Multi-step Interpolated-FFT procedure to the signal sets.

Based on the comparisons and discussions using numerical examples that resemble datasets of a 3D SLDV, it can be concluded that the proposed Multi-step Interpolated-FFT procedure can robustly improve the harmonic analysis accuracy for super-short sampled signals, allowing a significant reduction of testing time for a full-field measurement.

4. Application to a fan blade test

In this section, the proposed Multi-step Interpolated-FFT procedure is applied to the measured data of a generic fan blade. Firstly, pictures of the test set-up, the MISO vibration controller settings, and the 3D SLDV settings are introduced. Then two tests are carried out for the test structure: i) a conventional fast swept-sine test to quantify the degree of nonlinearity for the mode of interest and ii) a nonlinear phase resonance test in combination with 3D SLDV to perform a full-field measurement of the operating deflection shapes. Finally, the harmonic analysis process of the 3D SLDV datasets is elaborated, in which spectra of one representative scan point are illustrated before demonstrating the full-field, multi-harmonic operating deflection shapes.

4.1. Test set-up

In the test, the blade is clamped at the root using an appropriate clamping mechanism. As shown in Figure 15, the excitation system consists of a single-point force applied near the root of the blade by a Data Physics Signal Force V4 shaker and a MISO vibration controller (Data Physics SignalStar ABACUS Vector) [29]. The force signal is obtained via a force transducer (PCB 208C02). Three-directional responses of a reference point are recorded with a triaxial accelerometer (PCB 356A03) attached to the tip of the blade. Here, the accelerometer is used as a limit reference to ensure that the blade will not experience any excessive vibrations during the testing. It can be replaced by other non-contact transducers if necessary. The 3D SLDV used in this test is a Polytec PSV-500-3D-HV Scanning Laser Doppler Vibrometer [7].

Figure 16 shows the full-field measurement grid defined on the surface of the fan blade, which consisting of 2016 scan points. It also highlights the strong three-dimensional twisted shape of the blade, making the use of a 3D measurement system highly advisable. The coordinates of the scan points are precisely measured using the built-in geometry scan unit of 3D SLDV before the start of dynamic measurement. The response signals of three SLDV channels will be recorded by the 3D SLDV system only, while the input force signal is split to be measured by the 3D SLDV and the MISO vibration controller simultaneously.

This test was originally conducted for a technology demonstration in a University Technology Partnership meeting two years ago, where rectangular windows and anti-aliasing filters were used in the 3D SLDV acquisition settings. Note that, ideally, a 4-term Blackman Harris window should be applied here from the findings of this research, but it is impossible to change the window by post-processing the filtered data of 3D SLDV. Fortunately, the interference between the harmonics of the fan blade was not severe, such that the proposed procedure can still produce good results with the rectangular windowed spectra. All the experimental results have been normalised for the reason of commercial confidentiality.

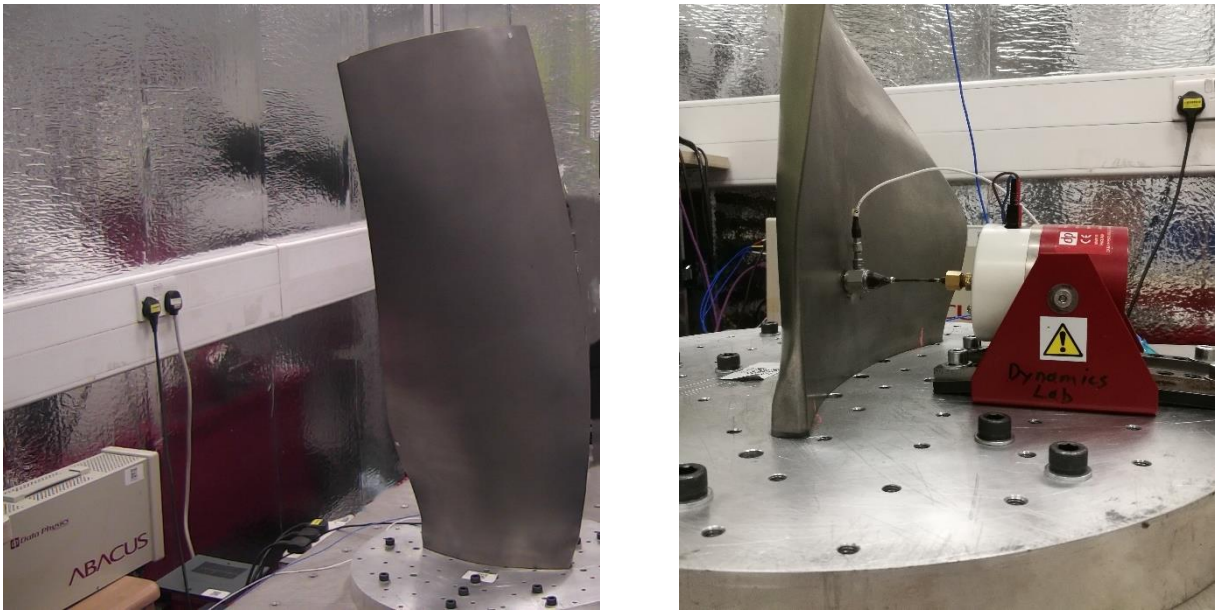

Figure 15. Test set-up: (a) front view and (b) side view.

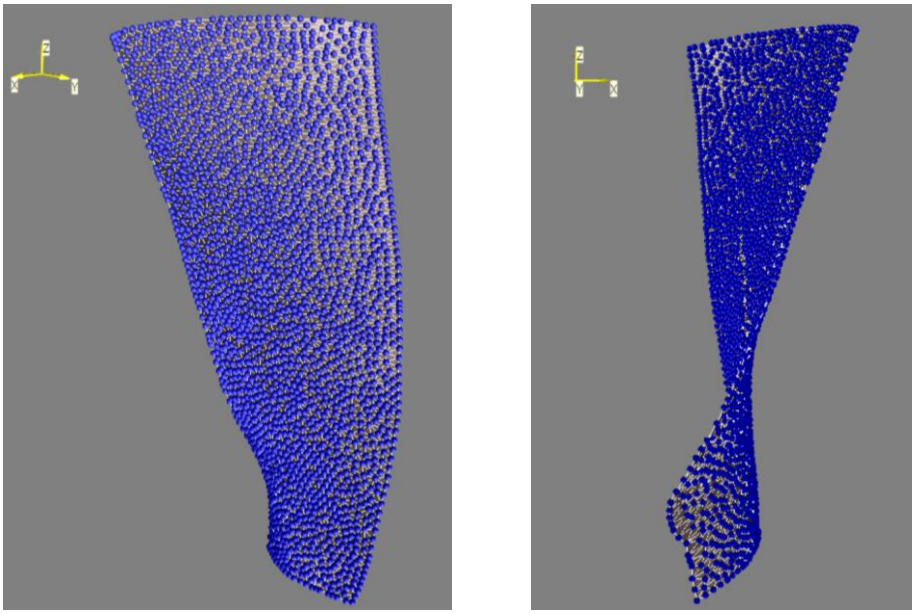

(a) (b)

Figure 16. A measurement grid of 2016 points: (a) front view and (b) side view provided by the Polytec Scan Viewer.

4.2. Fast swept-sine test

A conventional swept-sine test with different excitation levels is initially conducted using the MISO vibration controller. It aims to experimentally find the underlying linear properties for the mode of interest and quantify the degree

of nonlinearity of this mode. Five input forces, denoted as Level 1-5, are applied to the blade during the test. The force linearly sweeps the frequency within a very narrow bandwidth around the natural frequency of the investigated mode. In such a test, the MISO vibration controller applies a tracking filter when estimating frequency response functions; therefore, only the fundamental harmonic component of the response is provided by the controller, whereas the higher-order harmonics are filtered out by the controller.

Figure 17 shows the measured frequency responses of the blade tip in the fan blade's horizontal plane (x-direction and y-direction); the responses in the vertical axis (z-direction) are not shown here since they are too small. As can be seen, the structure demonstrates a typical softening behaviour within the investigated input levels: its resonant frequency gradually decreases with an increased level of forcing magnitude. Two definitions of backbone curves [30,31], i.e. a curve of maximal response amplitudes and a curve of phase lag quadrature points, are highlighted in the figures to capture the trend of the resonances. It is not surprising that these two backbone curves are very close to each other for the responses in both directions, as analytically derived in Ref [31]. However, it is interesting to see that the backbone curve of the phase lag quadrature points appears at the left side of the maximal response backbone curve for the responses in the x-direction, while it switches to the right side for the responses in the y-direction. As shown in the figure, a phase lag of approx. 5° is observed between the x- and y-directional responses, indicating non-proportional damping mechanisms of the fan blade test set-up. Five phase lag quadrature points of the x-directional responses - Resonance A' to Resonance E' - obtained by the swept-sine test are highlighted as red dots in Figure 17(a) and (b). Due to the well-known force-drop phenomenon [4], the actual forcing magnitude in a swept-sine test is generally lower than the nominal value (input levels 1-5, respectively). As such, Resonances A' to E' are only close approximates to the true phase resonances of the blade.

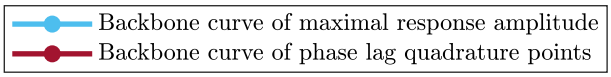

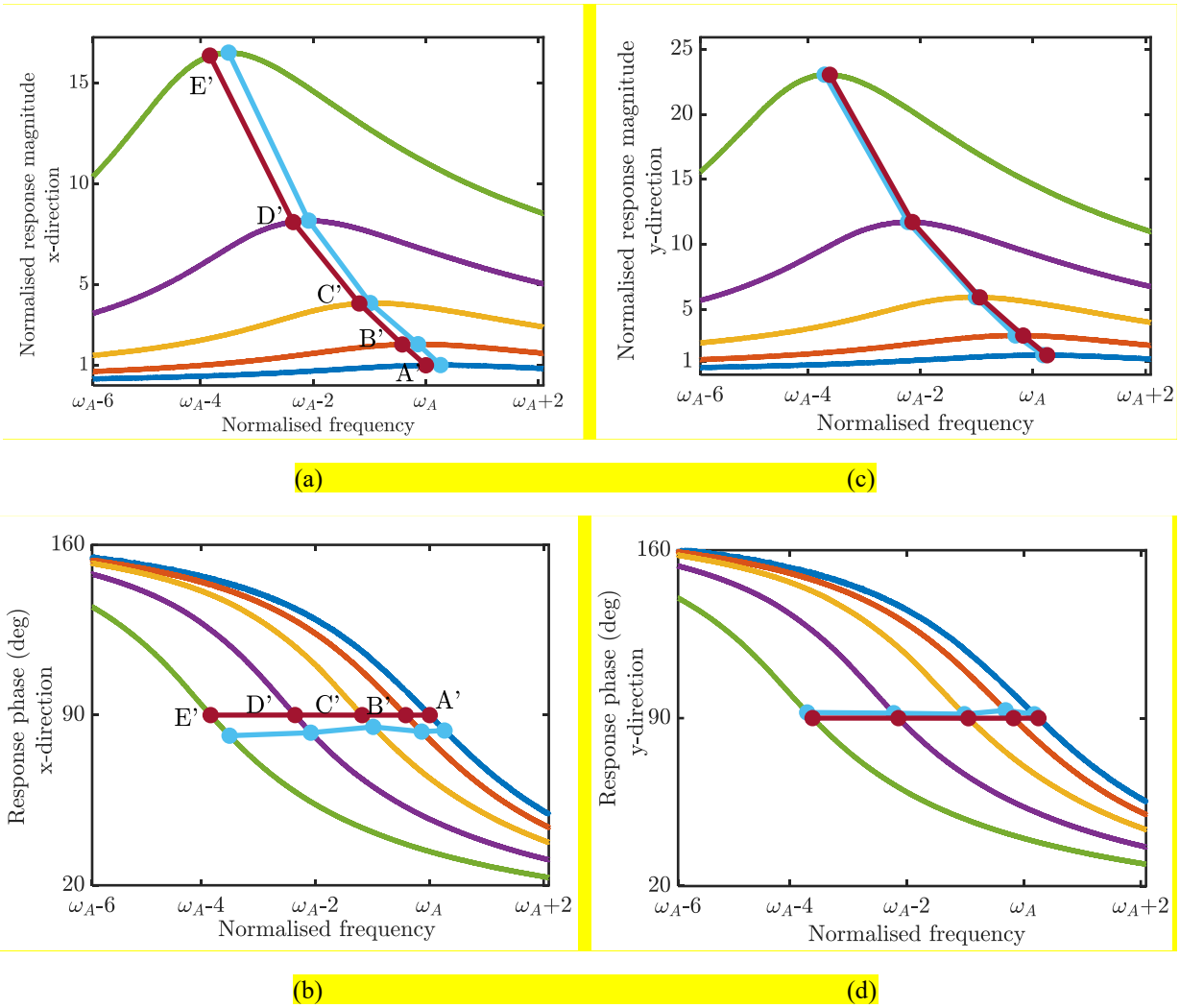

Figure 17. Measured accelerations of the blade tip in the fast swept-sine tests: (a) magnitude and (b) phase of the fundamental harmonic component of the response in the x-direction; (c) magnitude and (d) phase of the fundamental harmonic component of the response in the y-direction. Nominal input levels: — level 1, — level 2, — level 3, — level 4 and — level 5. Note that the magnitudes of responses are normalised using the peak value of Resonance A'.

4.3. Full-field phase resonance test

The nonlinear phase resonance test is then applied to the fan blade attempting to isolate one of its nonlinear modes [20-23]. A single-point, mono-harmonic sine-dwell force is used to keep the structure vibrating at resonant conditions by using an automatic resonance tracking module of the Data Physics SignalStar ABACUS Vector [29]. The criteria set for the sine-dwell control are two folds: first, the driving force is adjusted to have a phase lag of 90° with respect to the x-

directional acceleration of the blade tip within an accuracy of 1°. Secondly, the force amplitude is controlled to the required level (input level 1-5, respectively) with an accuracy of 0.1% to avoid any force drops. Accordingly, the that meet the criteria are herein named as Resonances A to E. As soon as the vibration controller dwells at a true phase resonance and reaches steady-state, the 3D SLDV (Polytec PSV-500-3D-HV) is used to measure the full-field vibration response of the blade. The sampling rate is set to 12.5 kHz, and a sampling interval of 0.32 s is chosen for each scan point to ensure that all 2016 points can be measured in approx. 11 minutes. To apply the Multi-step Interpolated-FFT procedure, the 3D SLDV datasets are exported to MATLAB using the Polytec file access software [32].

4.3.1. One representative scan point

The results of one representative scan point are used to illustrate the signal analysing process in detail. Figure 18 shows the conventional tapered-window spectra provided by 3D SLDV as blue dotted lines when the structure vibrates at Resonances A to E, respectively. A significant amount of short-range energy leakage and a coarse frequency resolution are visible from the spectra; this is expected due to a deliberate choice of a super-short sampling interval to reduce the testing time. The figures in the left column, i.e. Figure 18(a) to (e), illustrate the spectra of the input force signals, where only a single harmonic is visible, and no evident higher-order harmonics are observed. The figures in the right column (see Figure 18(f) to (j)) show the spectra of response signals, in which the fundamental harmonics dominate the responses. However, higher-order harmonics become non-trivial with increasing input force levels as nonlinear mechanisms are activated. It is also interesting to see that even harmonic components (e.g., second and fourth harmonic components) appear in the measured response spectra from input level 3 and above, which may be attributed to the asymmetrical geometry of the fan blade in a non-rotating configuration. Figure 18 also highlights the interpolated peaks by using the Multi-step Interpolated-FFT procedure, where the interpolation generally leads to a higher-magnitude estimation of the input force and the response signals compared to the estimates of the tapered-window FFT method. Therefore, the accuracy of the estimates of the two methods is further carefully evaluated in the following subsection.

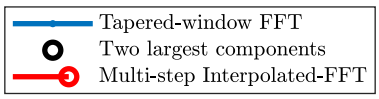

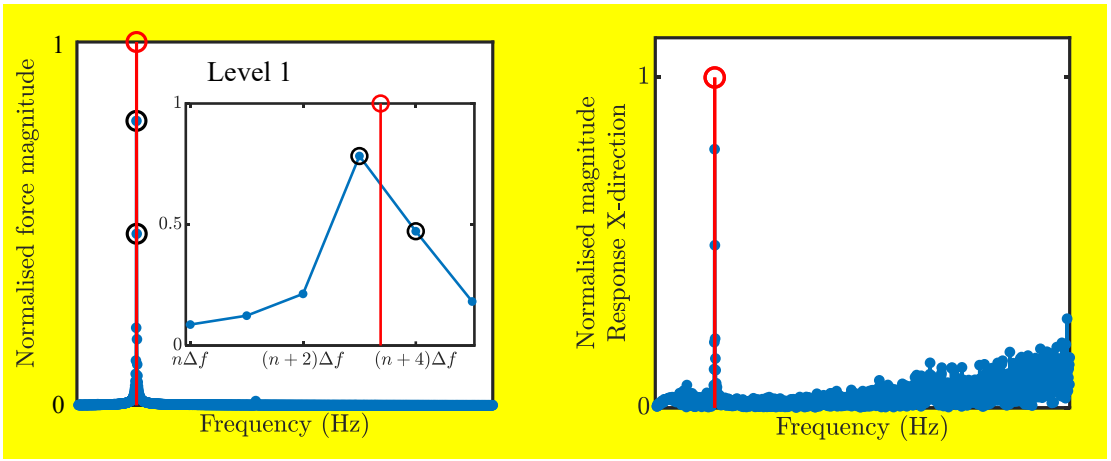
Level 1
Normalised force magnitude
Frequency (Hz)
$n\Delta f$
$(n+2)\Delta f$
$(n+4)\Delta f$
Normalised magnitude
Response X-direction
Frequency (Hz)

(a) (f)

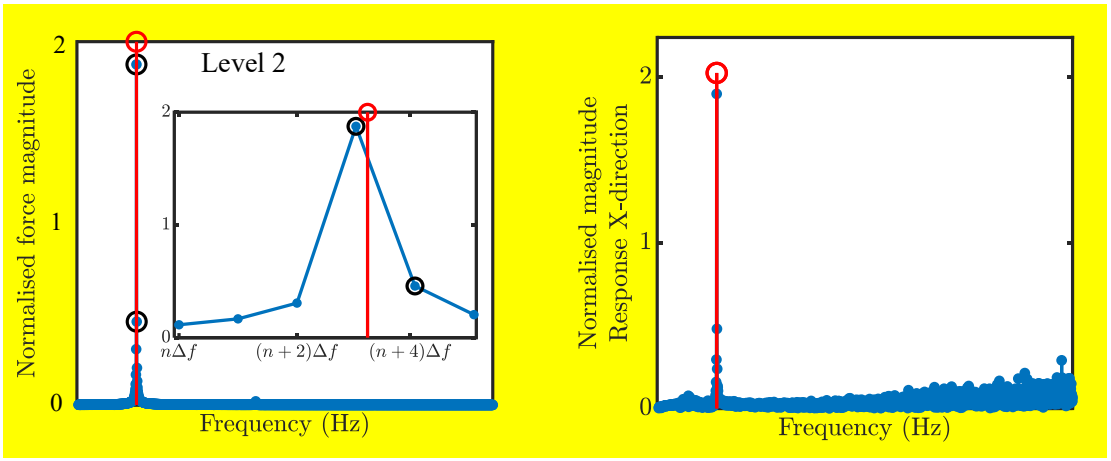
Level 2
Normalised force magnitude
Frequency (Hz)
$n\Delta f$
$(n+2)\Delta f$
$(n+4)\Delta f$
Normalised magnitude
Response X-direction
Frequency (Hz)

(b) (g)

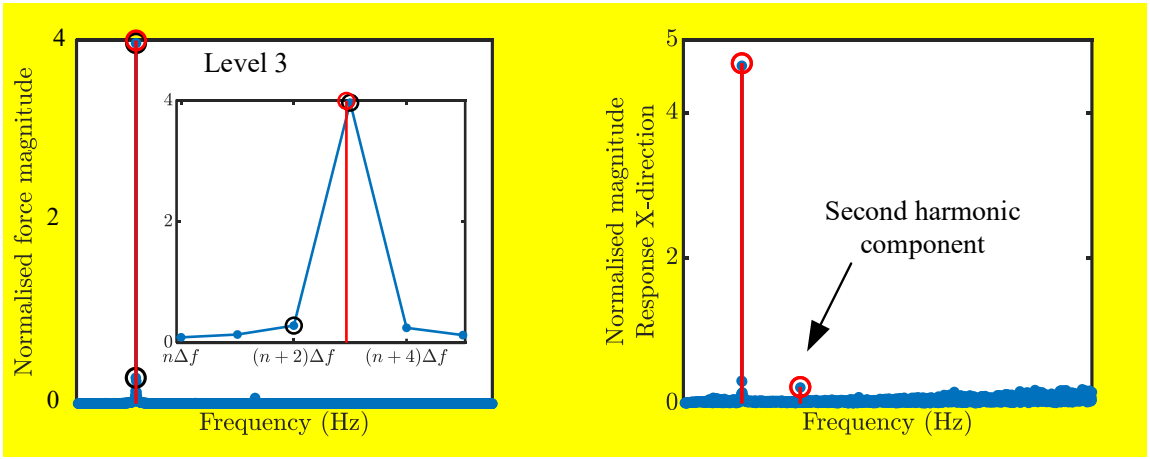
Level 3
Normalised force magnitude
Frequency (Hz)
$n\Delta f$
$(n+2)\Delta f$
$(n+4)\Delta f$
Normalised magnitude
Response X-direction
Second harmonic component
Frequency (Hz)

(c) (h)

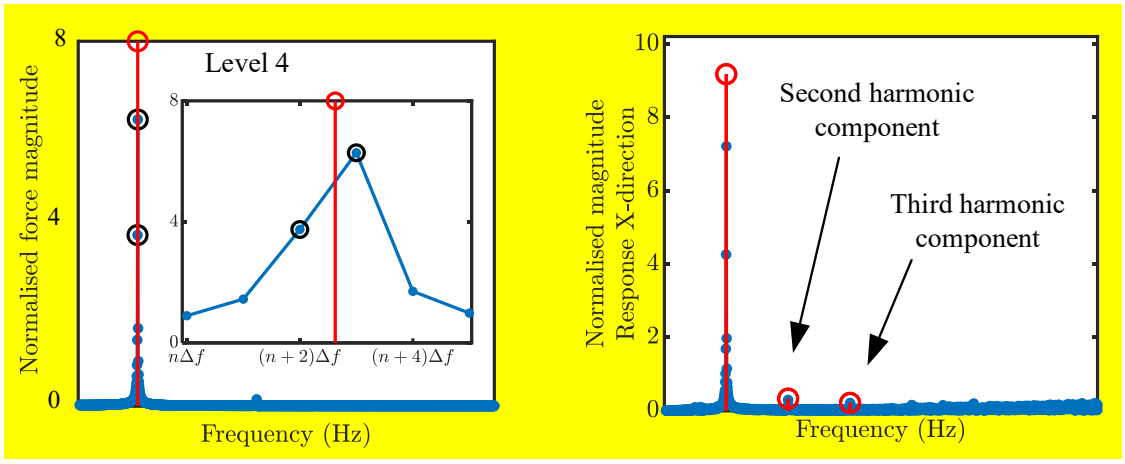

(d) (i)

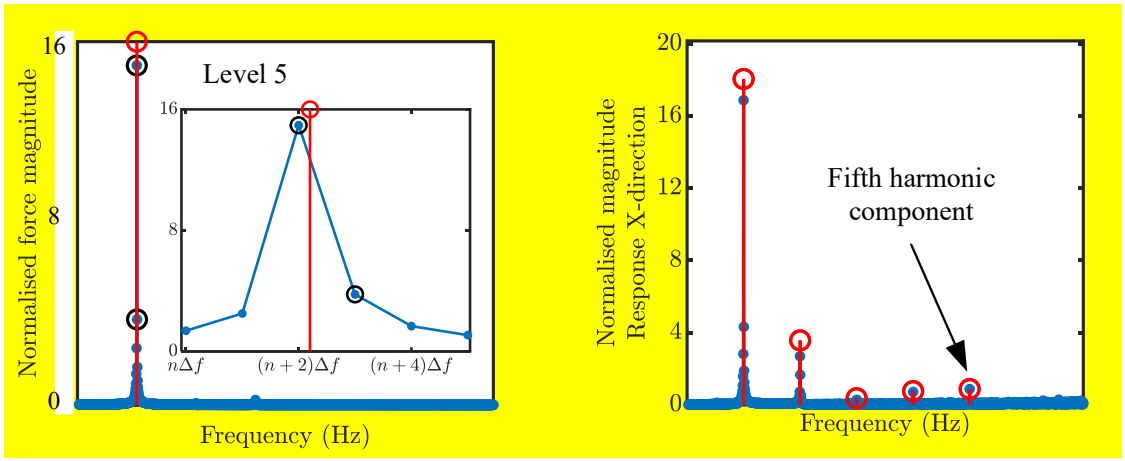

(e) (j)

Figure 18. Conventional tapered-window FFT method and Multi-step Interpolated-FFT procedure applied to the experimental dataset of one scan point. (a) to (e) illustrate the spectra of the driving force signal for Resonances A to E, respectively. Plots (f) to (j) depict the spectra of the accelerations in the x-direction for Resonances A to E, respectively. Note that the magnitudes of forces are normalised using the interpolated fundamental harmonic force of input level 1. Likewise, the magnitudes of responses are normalised using the interpolated fundamental harmonic response of Resonance A.

4.3.2. Validation using input force signals

As shown in Figure 1, the input force signals are recorded by the 3D SLDV in super-short segments and sampled by the MISO vibration controller with a much longer sampling interval. With such test settings, two instantaneous estimates of frequencies and amplitudes of the input forces can be obtained by applying the conventional tapered-window FFT

method and the Multi-step Interpolated-FFT procedure to 3D SLDV datasets, respectively. The results of these two harmonic analysis methods are now compared to the average estimates provided by the MISO vibration controller. Recall that the instantaneous estimates should not deviate too far away from the average estimates.

Figure 19 (a) compares the instantaneous estimates of the driving force magnitude for each scan point using the tapered-window FFT method against the average estimate provided by the MISO vibration controller. It is clearly shown that the tapered-window FFT method has a considerable amount of offsets due to spectral leakage. Only when the driving frequency is very close to one spectral line (see input level 3), the maximum relative magnitude difference can be as small as 0.75%; otherwise, deviations up to 22% (occurred at input level 1) can be encountered. Figure 19 (b) depicts the instantaneous estimates of the driving force magnitude using the Multi-step Interpolated-FFT procedure with respect to the average estimate. It is shown that the proposed procedure consistently provides a much more accurate estimation of the forcing magnitude regardless of its driving frequency: a maximum relative magnitude difference of only 0.025% (occurred at input level 5) is observed for all the scan points and for all the considered input levels. In this case, the proposed procedure is roughly three orders of magnitude more accurate than the tapered-window FFT method in estimating the driving force magnitudes.

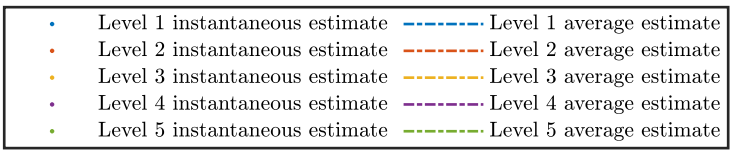

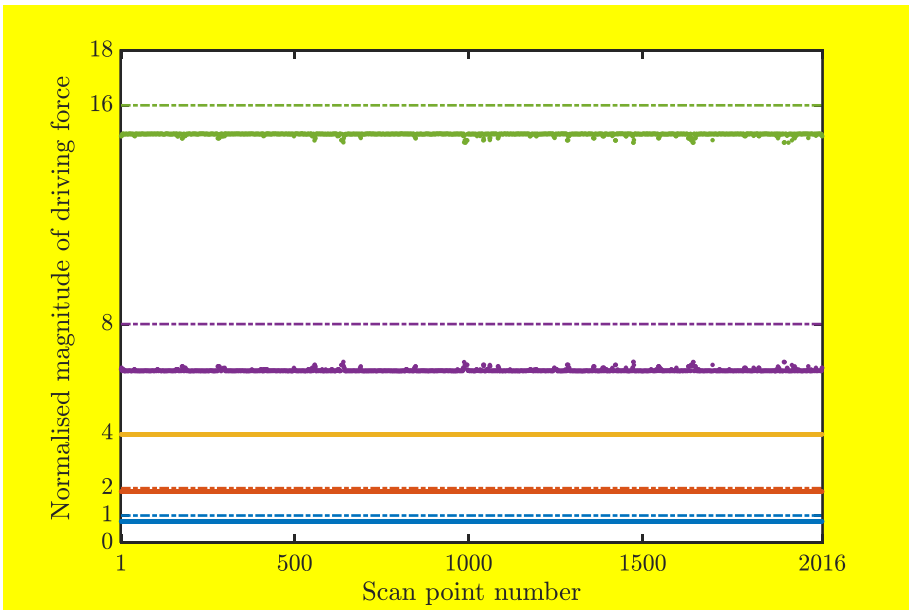

(a)

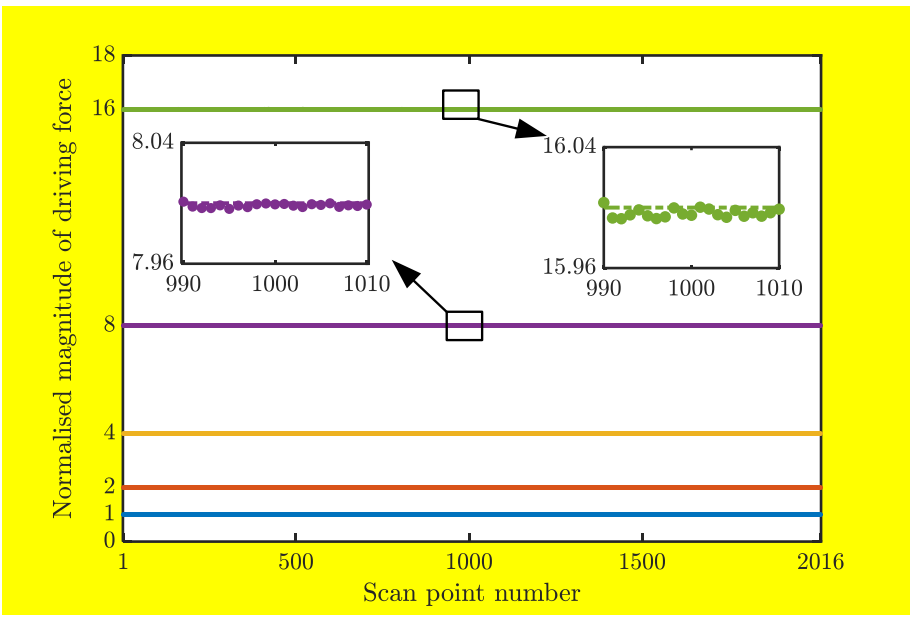

(b)

Figure 19. A comparison of average estimates of the input force provided by the MISO vibration controller and two instantaneous estimates by applying (a) the conventional tapered-window FFT method and (b) the proposed Multi-step Interpolated-FFT procedure to the 3D SLDV dataset.

Figure 20 (a) illustrates the instantaneous estimates of the driving frequency for each scan point using the tapered-window FFT method. Only two discrete frequencies can be estimated for the five input levels due to the coarse frequency

resolution (Δf =3.125 Hz). In contrast, Figure 20 (b) shows the instantaneous estimates of the driving force using the proposed procedure, where quite good agreement with the average estimates is reached. Only a maximum discrepancy of 0.125 Hz is observed for all the scan points and for all the input levels, which is at least an order of magnitude better than the tapered-window FFT method.

This subsection compares the accuracy of the two harmonic analysis methods using experimental data from the fan blade test. Excellent agreement is shown between the instantaneous estimates of the input force by applying the Multi-step Interpolated-FFT procedure and the average estimates from the MISO vibration controller. It confirms that the proposed procedure is quite effective in refining frequency resolution and improving estimation accuracy for signals featuring super-short sampling intervals. In the following sections, the tapered-window FFT spectra will only be used to determine the number of constituent harmonics in measured signal sets, while quantitative estimates of frequencies, amplitudes and phases of harmonics are performed by using the proposed procedure.

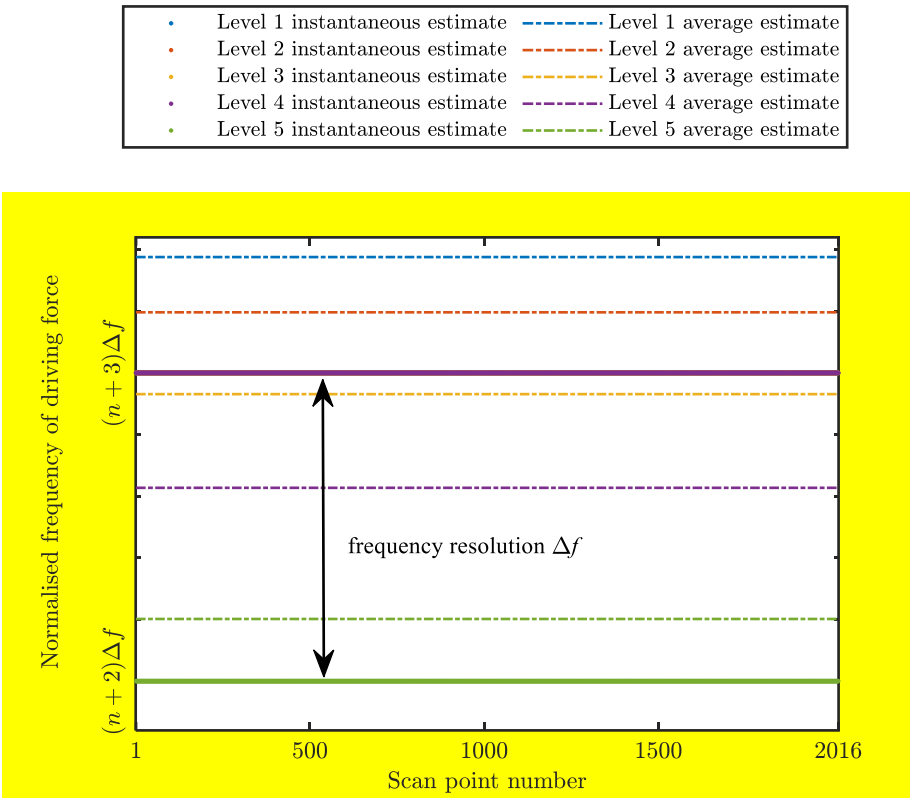

(a)

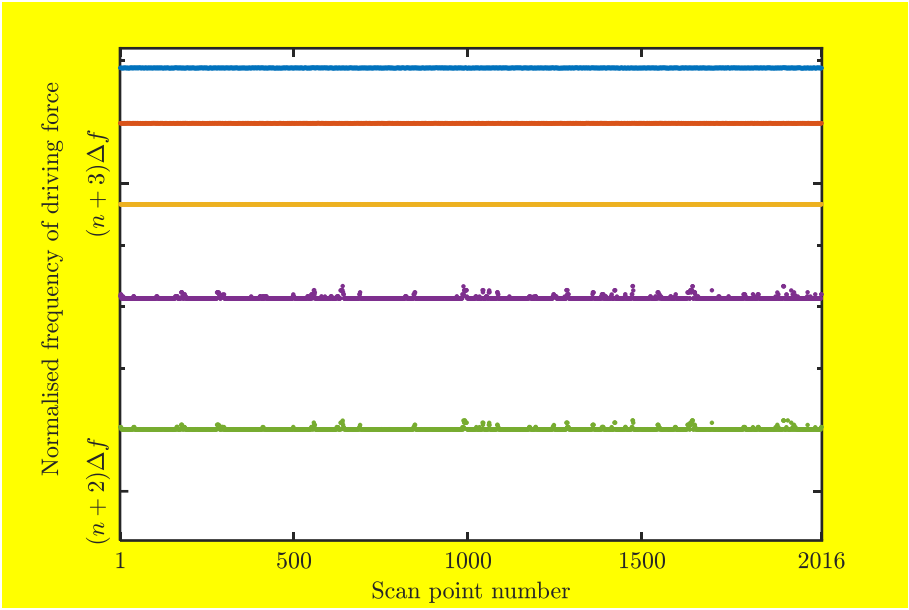

(b)

Figure 20. A comparison of average estimates of the driving frequency provided by the MISO vibration controller and two instantaneous estimates by applying (a) the conventional tapered-window FFT method and (b) the proposed Multi-step Interpolated-FFT procedure to the 3D SLDV datasets.

4.3.3. Quality of nonlinear mode isolation

After obtaining frequency, magnitude, and phase estimates of the fundamental harmonic of the full-field responses, the quality of the isolated nonlinear mode can now be assessed. This must be performed for a full-field measurement since the driving force is tuned in phase lag quadrature with only one point of the blade (a point near blade tip and measured by an accelerometer) using the MISO vibration controller. It is, therefore, in this subsection to assess whether the acceleration phase lags of scan points are also in phase quadrature with the input force. Another purpose of this assessment is to use the phase lags as criteria for removing points that may be considered outliers. This is also important for a 3D SLDV measurement since the datasets of some scan points can be unexpectedly poor and should be omitted for further analysis[19].

First, two magnitude thresholds for the full-field data are introduced:

- Upper magnitude limit: 5× RMS value of the vibration magnitudes of all scan points;

- Lower magnitude limit: RMS value of the vibration magnitudes of all scan points,

For the fan blade, the vibration magnitude for each scan point refers to its fundamental harmonic acceleration in the horizontal plane, i.e. $|A| = \sqrt{A_x^2 + A_y^2}$. Because the z-directional (axial) accelerations of the blade are found to be orders of magnitude smaller than those in the x- and y-directions, they are consequently not used in the data analysis. The practising engineer is advised to adjust the magnitude limits according to the quality of signals for individual problems.

Three categories are defined for scan points by using their accelerations in x- and y-directions:

1) *Phase quadrature points* represent the scan points that fulfil the phase lag quadrature criterion (within an accuracy of 10° to avoid oversensitivity) in both x- and y-directions. These points also vibrate smaller than the upper magnitude limit.

2) *Non-quadrature points* violate the phase lag quadrature criterion in x- or y-, or both directions, while the magnitudes of responses are smaller than the lower magnitude limit. The non-quadrature points often appear at locations with low SNR ratios, typically around nodal lines.

3) The rest of the scan points are considered *Outliers*. It includes two sub-groups: one group contains points that fail to comply with the phase lag quadrature criterion in x- or y-, or both directions but have sufficiently large magnitudes of vibration (larger than the lower magnitude limit). The other group contains points with suspiciously large response magnitudes, i.e. larger than the upper magnitude limit. The outliers are mainly caused by excessive speckle noises and often occur in structural areas with poor surface conditions, unwanted reflections, etc. These outlier results are rejected from further analysis, and their responses are replaced by the nearest point when plotting the figures.

Figure 21 illustrates the categories of scan points for Resonance E (input level 5), where the phase scatter diagrams in x- and y- directions are depicted in the right column. The figure clearly shows that most scan points are vibrating in phase quadrature with respect to the driving force (denoted as green markers), and the non-quadrature points (denoted as blue markers) are concentrated around nodal lines. Interested readers are referred to Appendix A for a complete list of phase scatter diagrams for other resonances.

As shown above, it is now confirmed that the appropriated force successfully isolates the nonlinear mode during the test. In addition, the Multi-step Interpolated-FFT procedure provides magnitude, frequency and phase lag estimates of the fundamental harmonic components of the full-field datasets with high accuracy.

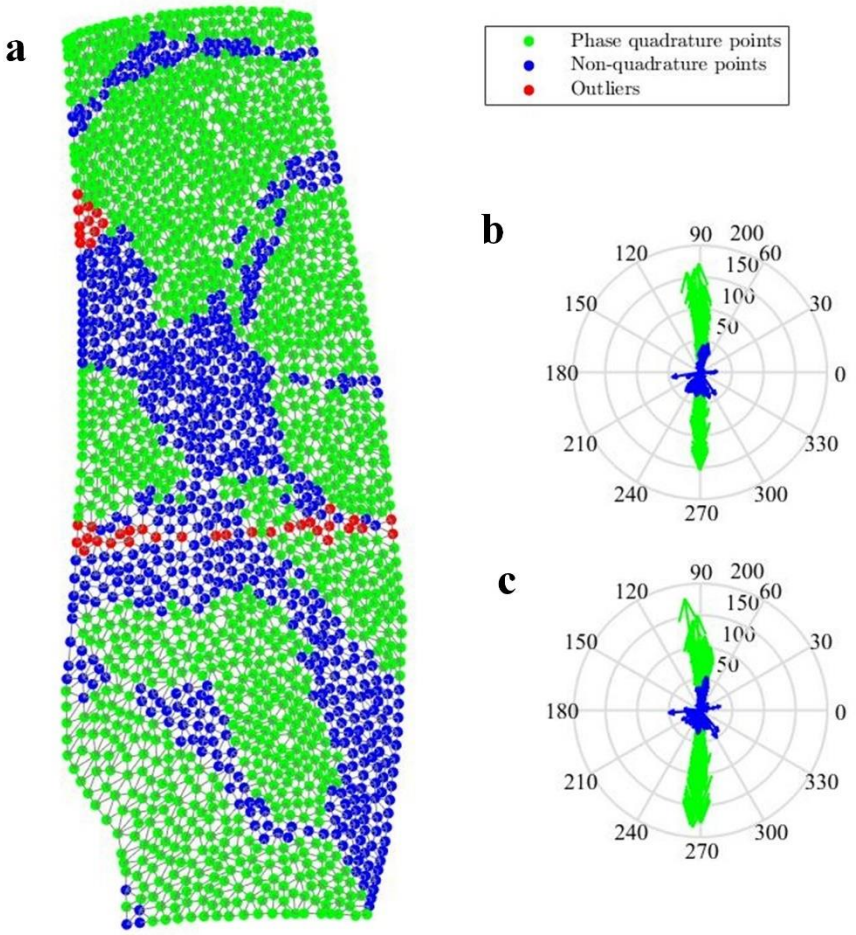

Figure 21. Full-field phase lags of accelerations for Resonance E: (a) mapping the indices onto the geometry of the scan points where green markers denote *phase quadrature points*, blue markers denote *non-quadrature points*, and the red markers denote *outliers*, respectively. Phase scatter diagrams of the fundamental harmonic component of the measured accelerations are shown in (b) x-direction and (c) y-direction, where datasets of the outliers are rejected.

4.3.4. Multi-harmonic, full-field operating deflection shapes

As accuracy of the proposed Multi-step Interpolated-FFT method is validated and high-quality nonlinear mode isolation is confirmed, the multi-harmonic, full-field operating deflection shapes for each resonance can now be plotted.

A. Number of harmonics

Since the operating deflection shapes of a nonlinear resonance may contain multiple harmonics, how many need to be included in the interpolation must be decided at this stage. Based on the datasets of phase quadrature points, two new indicators are introduced in this paper to describe the strength of each harmonic content - the Average Force Function (AFF) and the Average Response Function (ARF) - which are formulated using the tapered-window FFT spectra of the force and response signals, respectively.

$$AFF(\omega)=\frac{1}{N_{QP}}\sum_{N_{QP}}\left|F_i(\omega)\right|;\quad ARF(\omega)=\frac{1}{N_{QP}}\sum_{N_{QP}}\left|A_i(\omega)\right|, \tag{31}$$

where N_{QP} is the number of phase quadrature points, $F_i(\omega)$ and $A_i(\omega)$ denote the tapered-window FFT spectrum of the force and response signals for scan point *i*, respectively. $\left|A_i(\omega)\right|$ denotes the response magnitude in the horizontal plane (x- and y-directions) for the fan blade. As discussed earlier in Section 3, the tapered-window FFT spectra of 3D SLDV datasets only provide a coarse frequency resolution and unsatisfactory amplitude accuracy. Nevertheless, they should be good enough to determine the number of constituent harmonics here.

Figure 22 shows the results of AFFs and ARFs for Resonance E with a logarithmic scale of the y-axis, where a 2% line of the fundamental harmonic component is also highlighted in the figure. It is shown in Figure 22(a) that the AFF is indeed not a perfect mono-harmonic signal due to structure-shaker interactions. However, the magnitude of its higher-order harmonics never exceeds 2% compared to the fundamental harmonic, which confirms that strong interaction has been avoided in the phase resonance testing. Therefore, the input force can still be treated as a single sinusoid in this case. Figure 22(b) depicts the ARF concerning the responses in the horizontal plane, where several harmonics are observed exceeding the 2% threshold and therefore must be taken into consideration.

For other resonances, the AFF and ARF plots are detailed in Appendix B. The numbers of harmonics identified in the response signals are summarised in Table 5 for each resonance.

Table 5. The numbers of harmonics identified for each resonance using the Average Response Function.

Resonance index	Resonance A	Resonance B	Resonance C	Resonance D	Resonance E

Number of harmonics identified in the response signals	1,2,3,4	1,2,3,4,5,6	1,2,3,4,5,6	1,2,3,4,5,6	1,2,4,5,6

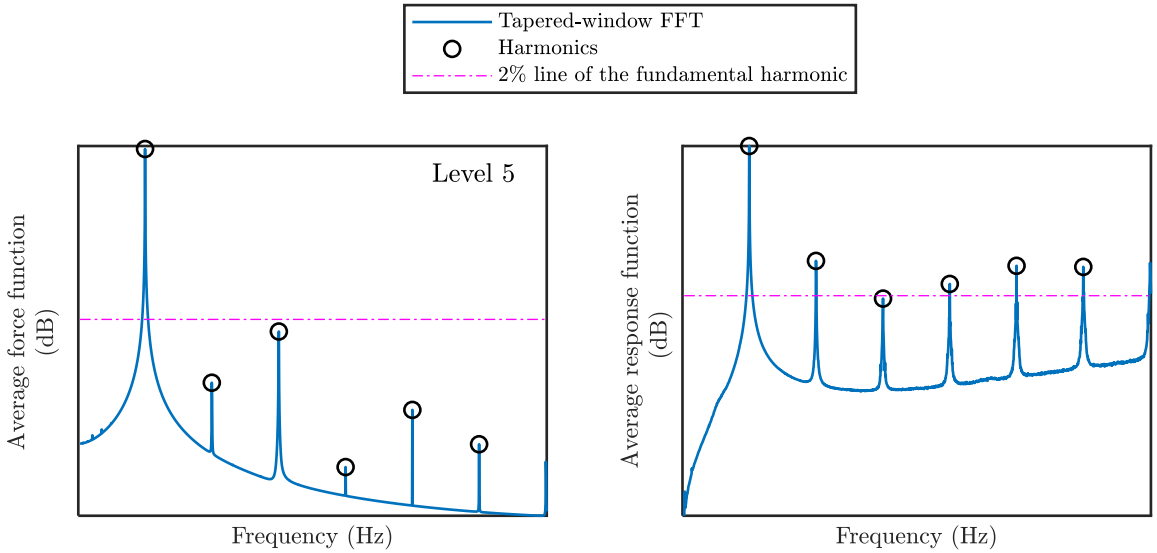

(a) (b)

Figure 22. The (a) average force function and (b) average response function for Resonances E.

B. Full-field operating deflection shapes

The full-field operating deflection shapes are then interpolated for each harmonic that has been identified as being of interest from the ARF plots. Table 6 shows the resulting operating deflection shapes for each harmonic and each resonance, where the colour represents the deformation amplitudes. It is shown that:

1) The full-field shape of the fundamental harmonic does not change significantly with increasing levels of input forces; this indicates that this mode of the fan blade is well separated from other modes, and no internal resonances are present in the datasets. In contrast, the deformation shapes of higher-order harmonics depend on the forcing level. For example, the second harmonic shape changes substantially for different input levels; this may be introduced by a broader shift of frequency for higher-order harmonics (a decrease of 4 Hz of the fundamental harmonic corresponding to an 8 Hz decrease of the second harmonic).

2) The deformation patterns for higher-order harmonics are much more complicated and harder to interpret than the lower-order harmonics, and their vibrations are becoming localised in small areas.

Table 6. Full-field operating deflection shapes for each harmonic and for each resonance of the fan blade.

Harmonic order	Resonance A	Resonance B	Resonance C	Resonance D	Resonance E
1st	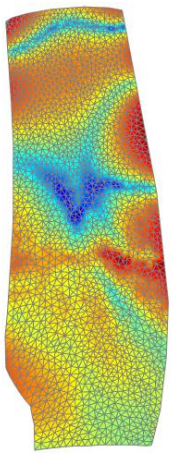	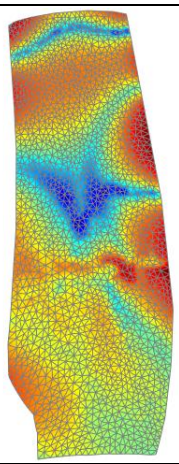	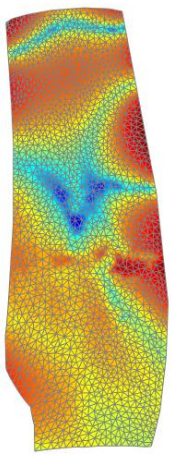	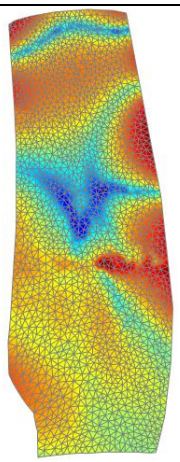	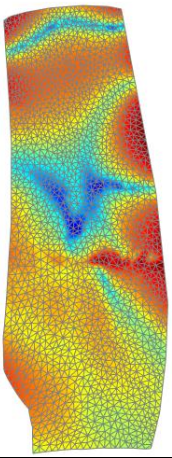
2nd	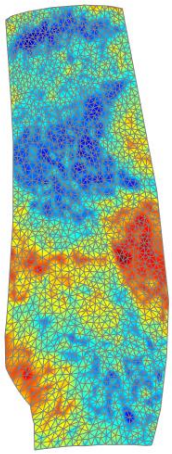	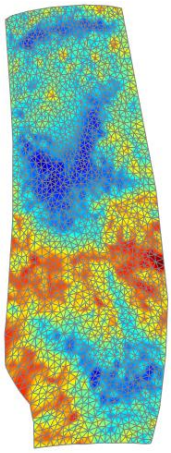	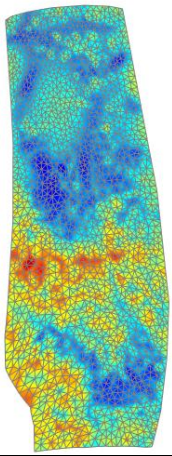	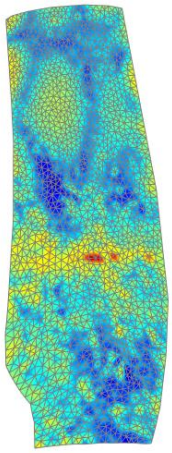	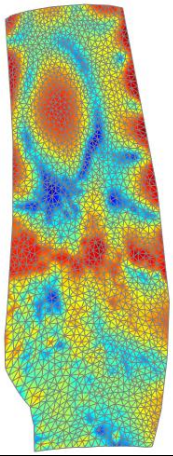
3rd	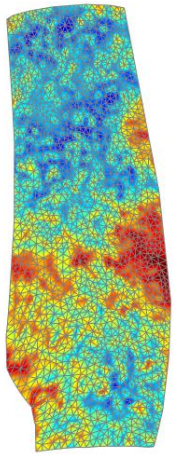	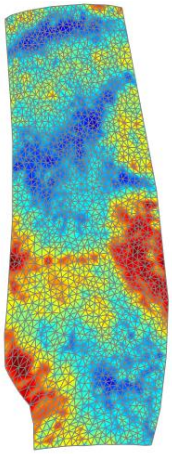	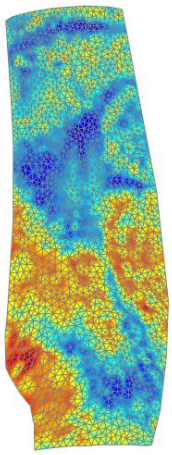	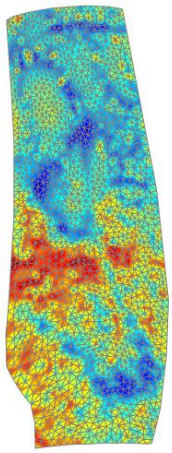	Non

Table 6 (continued)

Harmonic order	Resonance A	Resonance B	Resonance C	Resonance D	Resonance E
4th	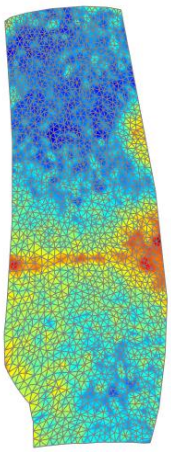	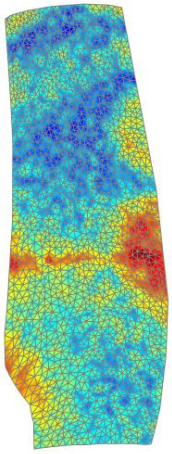	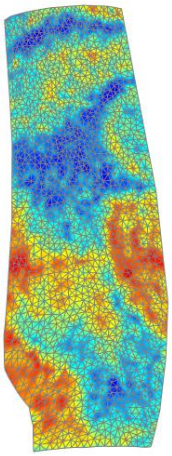	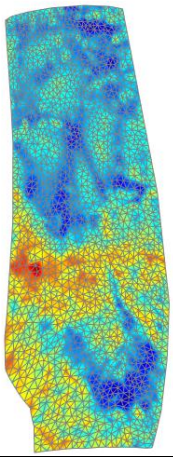	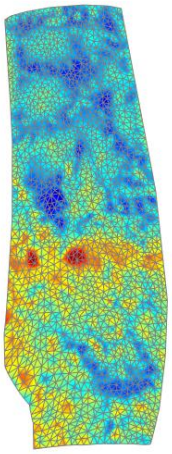
5th	Non	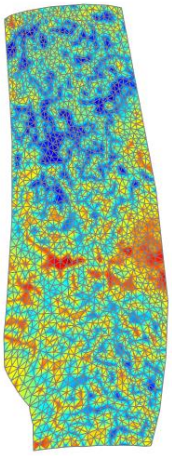	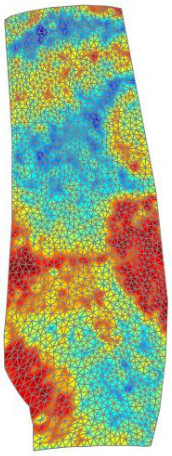	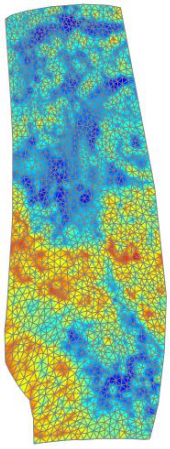	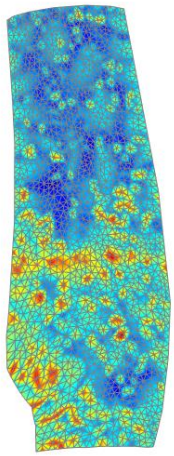
6th	Non	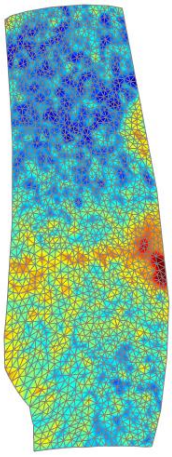	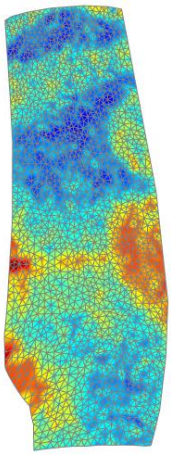	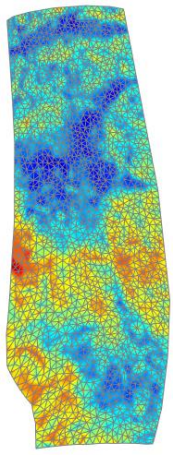	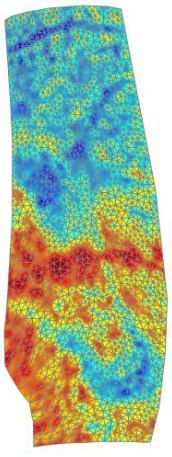

Finally, to ensure structural integrity during the high-amplitude phase resonance test, a second swept-sine test with the same input level as introduced in subsection 4.2 was conducted immediately after the phase resonance test. Again, only a minor change of 0.05 Hz of the resonant frequency was observed, which confirmed that the test set-up did not significantly change during the testing.

The results show that the multi-harmonic operating deflection shapes for a realistic nonlinear structure can be measured with an unprecedented resolution by using 3D SLDV and the proposed Multi-step Interpolated FFT procedure. A super-short sampling interval can be used for each scan point, thus requiring approx. 11 minutes for a full-field measurement of each resonance.

5. Conclusion and future perspectives

The presented research introduces a methodology to obtain full-field, multi-harmonic operating deflection shapes of nonlinear industrial-scale structures with 3D SLDV. A novel Multi-step Interpolated-FFT procedure combined with a phase resonance testing strategy has been developed to overcome some of the current issues with full-field nonlinear vibration testing, including long test duration, coarse frequency resolution, severe spectral leakage and spatial-inconsistent datasets. The procedure is initially explained in detail before it is demonstrated using three numerical examples. The numerical results show that the procedure can significantly refine the frequency resolution of super-short signals featuring multiple harmonics and provide accurate and robust estimations of harmonics present in the signal. The procedure is then applied to full-field nonlinear modal testing of a realistic fan blade. Significant improvement of estimation accuracy for the input force signals is seen when compared to the conventional tapered-window FFT method. A series of highly detailed, multi-harmonic deformation shapes of the fan blade is finally presented for different forcing levels, allowing, for the first time, to truly map and visualise individual harmonic components of resonant operating deflection shapes of an industrial-scale nonlinear structure.

The full-field measurement technique developed in this paper experimentally estimates the dynamic properties (such as natural frequencies, multi-harmonic operating deflection shapes at resonances) of a geometrically nonlinear structure with high confidence. Therefore, model updating algorithms that take these harmonics into the objective function can be developed. Moreover, the spatially-detailed operating deflection shapes are advantageous in describing local deformation patterns of nonlinear structures, allowing essential ingredients in model updating algorithms, such as the Modal Assurance Criterion (MAC) values, to be correlated with exceptionally high quality.

Acknowledgement

The authors thank Rolls-Royce plc and the EPSRC for the support under the Prosperity Partnership Grant\Cornerstone: Mechanical Engineering Science to Enable Aero Propulsion Futures, Grant Ref: EP/R004951/1. Further, would the authors like to thank Dr. L. Muscutt for his support with the test set-up. X.W. also recognise the support from Sun Yat-Sen University with a contract number of 76200-18841240 and the support from the National Natural Science Foundation of China under Grants 52005522 and 12072378.

Appendix A. Phase scatter diagrams of Resonances A to D

The full-field accelerations of the fan blade are measured using a 3D SLDV, where the coordinates are shown in Figure 16. The fundamental harmonic of the accelerations in the horizontal plane (x- and y-directions) are then estimated by using the Multi-step Interpolated-FFT procedure, where the phase scatter diagrams for Resonances A to D (highlighted in Figure 18) are listed as follows:

(1) Resonance A

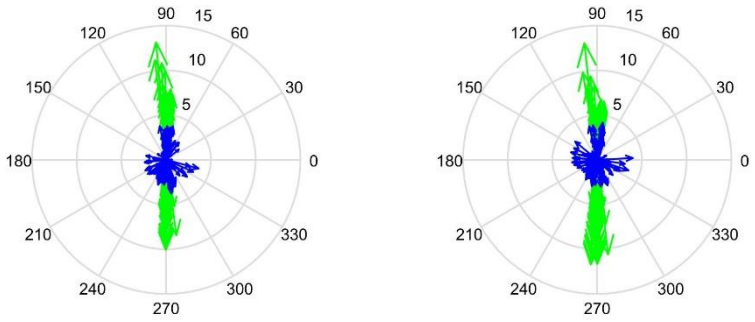

(a) (b)

Figure 23. Phase scatter diagrams of scan points for Resonance A in (a) x-direction and (b) y-direction.

(2) Resonance B

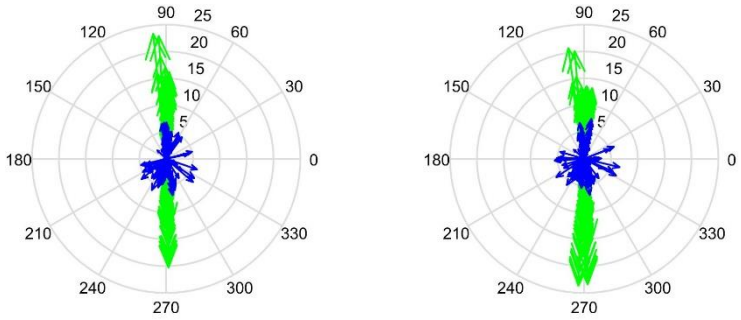

(a) (b)

Figure 24. Phase scatter diagrams of scan points for Resonance B in (a) x-direction and (b) y-direction.

(3) Resonance C

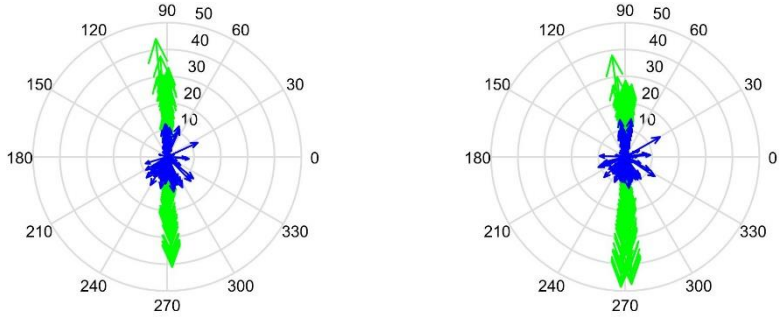

(a) (b)

Figure 25. Phase scatter diagrams of scan points for Resonance C in (a) x-direction and (b) y-direction.

(4) Resonance D

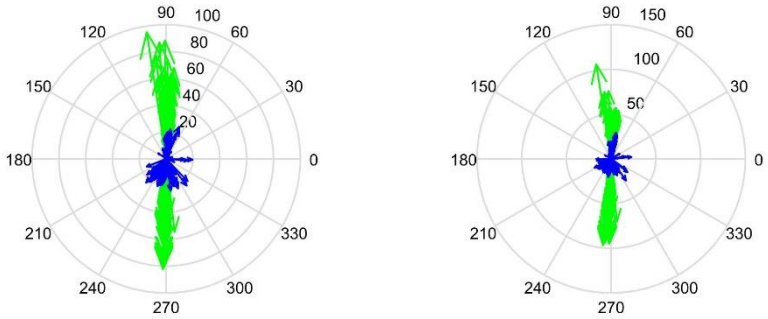

(a) (b)

Figure 26. Phase scatter diagrams of scan points for Resonance D in (a) x-direction and (b) y-direction.

Appendix B. Average Force Functions and Average Response Functions

The average force function and average response function defined by Eq. (31) are calculated from the tapered-window FFT spectra of the force and response signals in 3D SLDV datasets, where datasets of phase quadrature points (defined in Subsection 4.3.2) are used. For Resonances A to D (highlighted in Figure 18), they are shown as follows:

(1) Resonance A

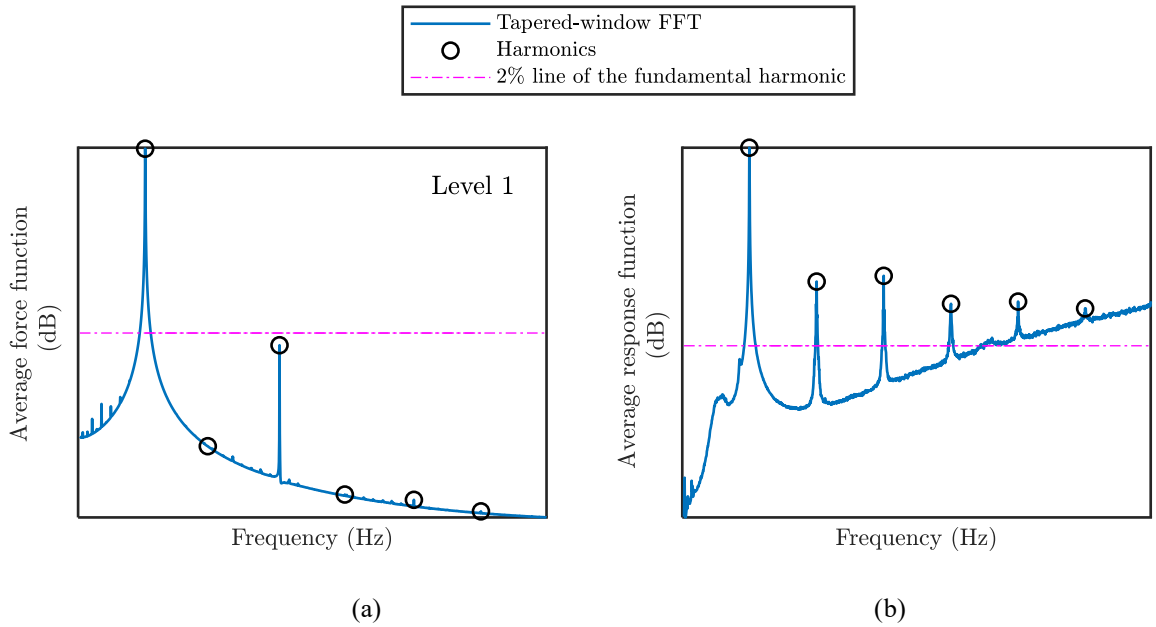

Figure 27. The (a) average force function and (b) average response function for Resonance A.

(2) Resonance B

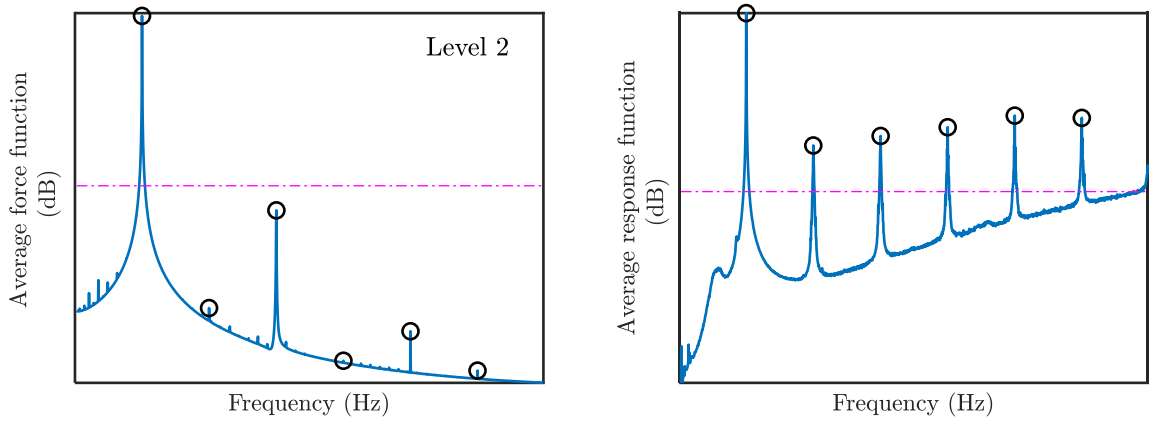

(a) (b)

Figure 28. The (a) average force function and (b) average response function for Resonance B.

(3) Resonance C

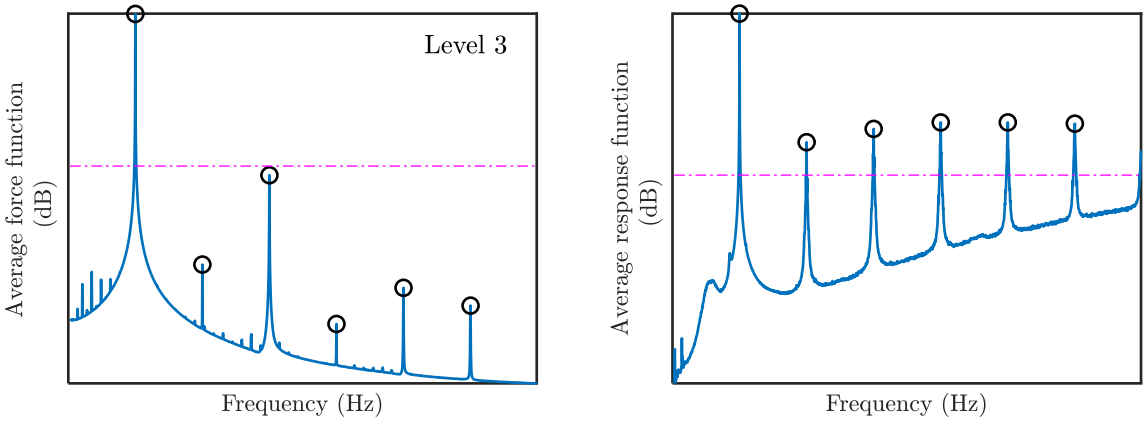

(a) (b)

Figure 29. The (a) average force function and (b) average response function for Resonance C.

(4) Resonance D

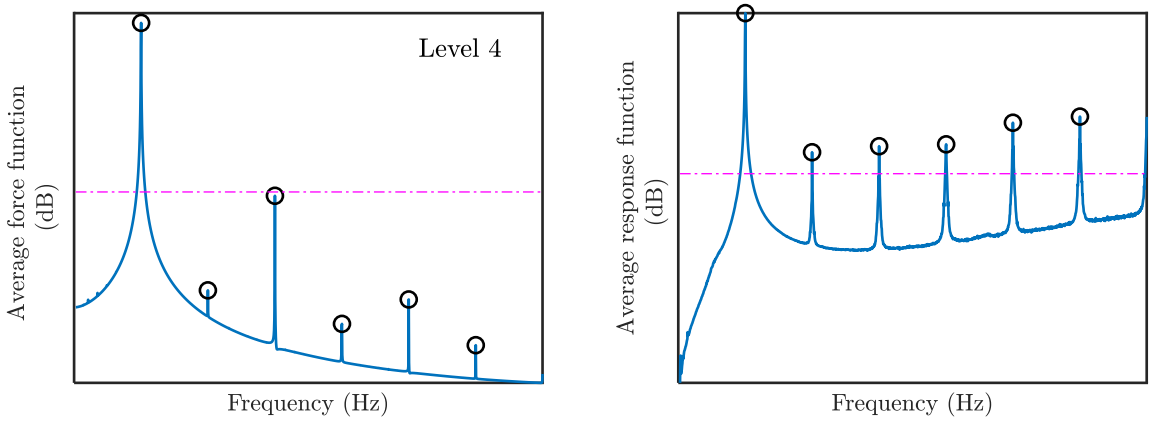

(d) (i)

Figure 30. The (a) average force function and (b) average response function for Resonance D.

References

[1] Maguire, Martyn, and Ibrahim Sever. Full-field strain measurements on turbomachinery components using 3D SLDV Technology. AIP Conference Proceedings. Vol. 1740. No. 1. AIP Publishing, 2016.

[2] Sever, I. A., and M. Maguire. Correlation of Full-Field Dynamic Strain Measurements with Reverse Engineered Finite Element Model Predictions. Experimental Techniques, 2021, 1-11.

[3] Kerschen, G., Worden, K., Vakakis, A. F., & Golinval, J. C. Past, present and future of nonlinear system identification in structural dynamics. Mechanical systems and signal processing, 2006, 20(3), 505-592.

[4] Ewins, David J. Modal testing: theory and practice,1986, 109-110.

[5] Ehrhardt, D. A., Allen, M. S., Yang, S., & Beberniss, T. J. Full-field linear and nonlinear measurements using continuous-scan laser doppler vibrometry and high speed three-dimensional digital image correlation. Mechanical Systems and Signal Processing, 2017, 86: 82-97.

[6] Ehrhardt, D. A., Allen, M. S., Beberniss, T. J., & Neild, S. A. Finite element model calibration of a nonlinear perforated plate, Journal of Sound and Vibration, 2017, 392: 280-294.

[7] Rothberg, S. J., et al. An international review of laser Doppler vibrometry: Making light work of vibration measurement, Optics and Lasers in Engineering, 2017, 99: 11-22.

[8] Di Maio, D., et al. Continuous Scanning Laser Vibrometry: A raison d'être and applications to vibration measurements. Mechanical Systems and Signal Processing,2021, 156: 107573.

[9] Polytec. Polytec user manual – Vibrometer controller OVF 5000.

[10] Vuye, C., Vanlanduit, S., Presezniak, F., Steenackers, G., & Guillaume, P. Optical measurement of the dynamic strain field of a fan blade using a 3D scanning vibrometer. Optics and Lasers in Engineering, 2011, 49(7): 988-997.

[11] Oliver, David E., and Matthias Schuessler. Automated robot-based 3d vibration measurement system, Sound & Vibtaion, 2009, 43(4): 12-15.

[12] Wollmann, T., et al. Combined Experimental-Numerical Approach for the 3D Vibration Analysis of Rotating Composite Compressor Blades: An Introduction, 18th European Conference on Composite Materials, Athens, Greece, 2018 June 24-28th.

[13] Chen, Yuanchang, Dagny Joffre, and Peter Avitabile, Underwater dynamic response at limited points expanded to full-field strain response, Journal of Vibration and Acoustics, 2018, 140(5): 051016.

[14] Jain, Vijay K., William L. Collins, and David C. Davis, High-accuracy analog measurements via interpolated FFT. IEEE Transactions on Instrumentation and Measurement, 1979, 28(2): 113-122.

[15] Grandke, Thomas. Interpolation algorithms for discrete Fourier transforms of weighted signals. IEEE transactions on instrumentation and measurement, 1983, 32(2): 350-355.

[16] Andria, Gregorio, Mario Savino, and Amerigo Trotta. Windows and interpolation algorithms to improve electrical measurement accuracy. IEEE Transactions on Instrumentation and Measurement, 1989, 38(4): 856-863.

[17] Zhang, Fusheng, Zhongxing Geng, and Wei Yuan. The algorithm of interpolating windowed FFT for harmonic analysis of electric power system. IEEE transactions on power delivery, 2001, 16(2): 160-164.

[18] Harris, Fredric J. On the use of windows for harmonic analysis with the discrete Fourier transform. Proceedings of the IEEE, 1978, 66(1): 51-83.

[19] Zanarini, Alessandro. Competing optical instruments for the estimation of Full Field FRFs. Measurement, 2019, 140: 100-119.

[20] Peeters, Maxime, Gaëtan Kerschen, and Jean-Claude Golinval. Dynamic testing of nonlinear vibrating structures using nonlinear normal modes. Journal of Sound and Vibration 2011, 330(3): 486-509.

[21] Peter, Simon, and Remco I. Leine. Excitation power quantities in phase resonance testing of nonlinear systems with phase-locked-loop excitation. Mechanical Systems and Signal Processing, 2017, 96: 139-158.

[22] Renson, L., Shaw, A. D., Barton, D. A., & Neild, S. A. Application of control-based continuation to a nonlinear structure with harmonically coupled modes. Mechanical Systems and Signal Processing, 2019,120: 449-464.

[23] Schwarz, S., Kohlmann, L., Hartung, A., Gross, J., Scheel, M., & Krack, M. Validation of a turbine blade component test with frictional contacts by phase-locked-loop and force-controlled measurements. Journal of Engineering for Gas Turbines and Power, 2020,142(5): 051006.

[24] Duda, K. DFT interpolation algorithm for Kaiser–Bessel and Dolph–Chebyshev windows. IEEE Transactions on Instrumentation and Measurement, 2011, 60(3): 784-790.

[25] Ifeachor, Emmanuel C., and Barrie W. Jervis. Digital signal processing: a practical approach. Pearson Education, 2002.

[26] Dynamic Signal Analysis Review: Part 3 – Aliasing. https://blog.dataphysics.com/dynamic-signal-analysis-review-aliasing/

[27] Zanarini, Alessandro. Competing optical instruments for the estimation of Full Field FRFs. Measurement, 2019, 140: 100-119.

[28] https://de.mathworks.com/help/matlab/ref/rand.html.

[29] https://www.dataphysics.com/products-and-solutions/vibration-controllers-signalstar/signalstar-vector.html

[30] Hill, T. L., Cammarano, A., Neild, S. A., & Wagg, D. J. Interpreting the forced responses of a two-degree-of-freedom nonlinear oscillator using backbone curves. Journal of Sound and Vibration, 2015, 349, 276-288.

[31] Breunung, Thomas, and George Haller. Explicit backbone curves from spectral submanifolds of forced-damped nonlinear mechanical systems. Proceedings of the Royal Society A: Mathematical, Physical and Engineering Sciences, 2018, 474(2213): 20180083.

[32] https://www.polytec.com/eu/vibrometry/products/software/fileaccess/